1964

Construction and test of equipment for use in ultrasonic pulse echo studies.

Charles Joseph Reinheimer

CONSTRUCTION AND TEST OF EQUIPMENT FOR USE IN ULTRASONIC PULSE ECHO STUDIES

by

CHARLES JOSEPH REINHEIMER, 1939-

A

THESIS

submitted to the faculty of the

SCHOOL OF MINES AND METALLURGY OF THE UNIVERSITY OF MISSOURI

in partial fulfillment of the requirements for the

Degree of

MASTER OF SCIENCE, PHYSICS MAJOR

Rolla, Missouri

1964

Approved by

Charles H. McDaniel (advisor) H. L. Leighly Jr.,

Charles E. Gotlb F. B. Pauls

TABLE OF CONTENTS

LIST OF ILLUSTRATIONS

LIST OF ILLUSTRATIONS

LIST OF TABLES

ABSTRACT

An ultrasonic pulse generator was constructed with a variable pulse width ranging from 4 microseconds to 10 milliseconds and a repetition period varying from 15 milliseconds to 5 seconds. The oscillator had an almost continuous range from 500 kilocycles to 18 megacycles per second.

Its applicability in studies of internal friction of metals was demonstrated with a single crystal aluminum sample.

ACKNOWLEDGEMENT

The author would like to express his thanks and appreciation to his advisor, Dr. Charles E. McFarland, for his guidance and assistance in the completion of this thesis.

A special note of appreciation is extended to Mr. Edward Stepp for his informative discussions and help with regard to the electronic apparatus.

I. INTRODUCTION

The use of ultrasonic waves, consisting of frequencies above 20,000 cycles per second, has risen to a high degree of popularity in both research and practical applications. The pulsed ultrasonic wave, employing echo techniques, has proved its use in attenuation and velocity studies of liquids, gases and solids.

The importance of the ultrasonic pulse generator as applied to the studies of attenuation in solids is expressed excellently by Granato and Lücke (1). They state that the possibility of gathering information regarding the behavior of dislocations in internal friction studies by the use of the ultrasonic pulse method seems to have been overlooked. One advantage of this method is that data regarding the frequency dependence of the internal friction, which can be important in determining the validity of existing theories, can be made in the range from 3 to 300 megacycles per second.

The purpose of this research was twofold. First, as an ultrasonic pulse generator was not available in this laboratory, the construction of such apparatus, employing a wide range of frequencies, a variable pulse width and repetition rate, was necessary. Such a device allows research to be conducted in fields other than that considered here.

Second, this work was concerned with demonstrating that with this apparatus, echoes can be obtained in a single crystal of aluminum. From these echoes, it is possible to obtain a measurement of the internal friction of the metal. These measurements, in turn, can be utilized to verify existing theories of internal friction. One such theory is that of Granato and Lücke (2), which predicts a definite dependence or

the internal friction on the frequency of the ultrasonic pulse.

Niblett and Wilks (3) point out in their review article on internal friction, that various frequency dependences have been found experimentally. A more detailed description of the theoretical frequency dependence of the Granato and Lücke theory and previous experimental results are given in the section entitled REVIEW OF LITERATURE.

II. REVIEW OF LITERATURE

It has been observed that if any form of mechanical vibration is applied to a metal sample, the vibration of the sample decreases exponentially to zero after the applied vibration is discontinued. The phenomena which account for this absorption of energy are called collectively the internal friction. The internal friction, $1/Q$, is related to the logarithmic decrement, Δ, by

$$\Delta = \pi/Q \tag{2.1}$$

The logarithmic decrement in turn, is defined as

$$\Delta = \Delta W/2W \tag{2.2}$$

where W is the total vibrational energy of the specimen, exclusive of thermal vibrations, and ΔW is defined as the energy loss per cycle.

A theory which has received much attention in trying to account for the source of this internal friction is based on the presence of dislocations in the lattice. Essentially, dislocations can be divided into two classes, edge dislocations and screw dislocations, with the edge dislocation being of main concern here. This discussion of edge dislocations is based on similar material from Seitz (4), Kittel (5) and Read (6).

One of the basic definitions encountered in working with dislocations is that of the Burgers vector. Given a cube of material, as shown in Figure 1, it can be sliced so that a surface S, bounded by a closed curve C, is formed. Now imagine the atoms on one side of the surface to be displaced a vector distance $\vec{d}$ by some applied force.

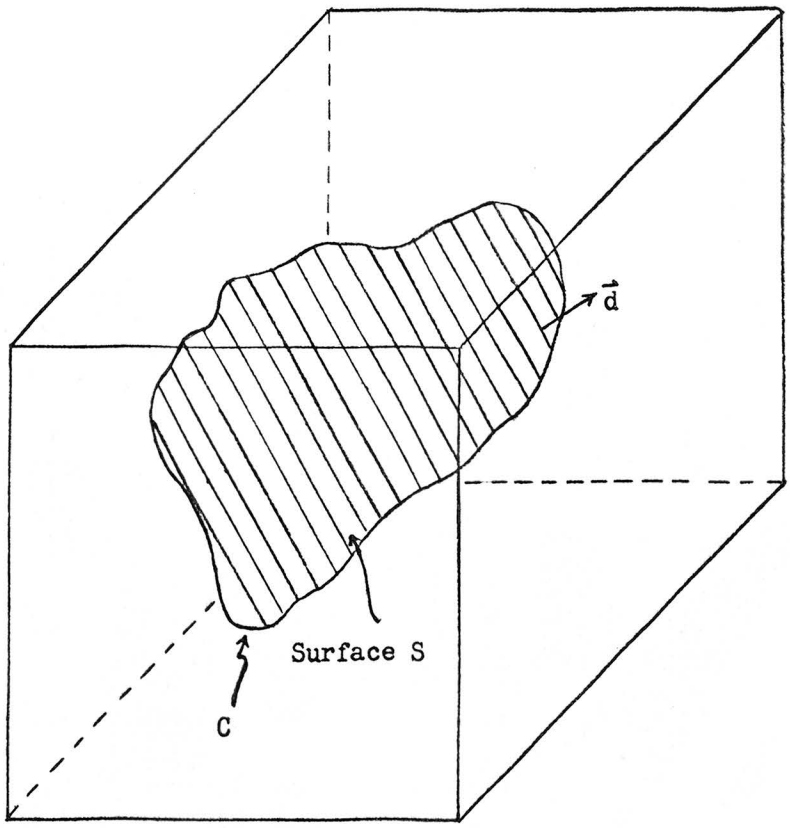

Fig. 1. Model for defining Burgers vector.

If $\vec{d}$ is not parallel to the cut surface, this relative displacement will cause either a gap or an overlap to be formed between the two halves of the cut surface. This can be corrected by either the addition or removal of atoms, depending on whether a gap or an overlap is created. The material is then rejoined and the original displacing force relaxed. The result is a strain in the crystal as a consequence of the relative displacement. C then forms what is known as a dislocation ring, and $\vec{d}$ being called the Burgers vector. This displacement need not be parallel to the surface, S, but if it is, S is called the slip plane, and d for most practical purposes is the edge of a unit cell and in the direction of slip.

Consider now a normal array of atoms in a crystal lattice, as shown in Figure 2. If slip occurs in one of the planes of atoms, that is if the atoms of one plane move relative to those in an adjacent plane, the result is an edge dislocation as shown in Figure 3. Note that slip has occurred in only part of the slip plane, for if all atoms had been displaced the same amount, the resulting lattice structure would be identical to the original structure. This type of dislocation derives its name "edge" because of the extension of a row of atoms at the side of the cubic lattice due to the slipping process.

This same sort of figure could be obtained by introducing an extra vertical plane of atoms at the center of the top half of Figure 2. Hence it can be seen that the lattice is under compression in the upper half plane and tension in the lower half plane.

Figure 3 can be thought of as a cross section of Figure 4, with DA corresponding to an edge of a plane in Figure 4. The plane formed by DABC corresponds to the surface S in Figure 1 and is called the

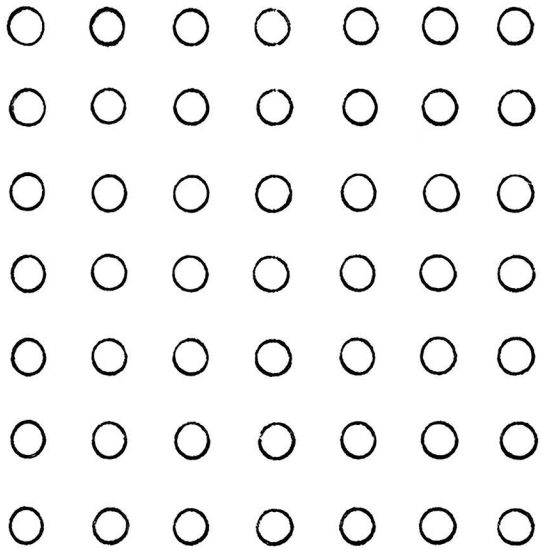

Fig. 2. Normal crystal lattice.

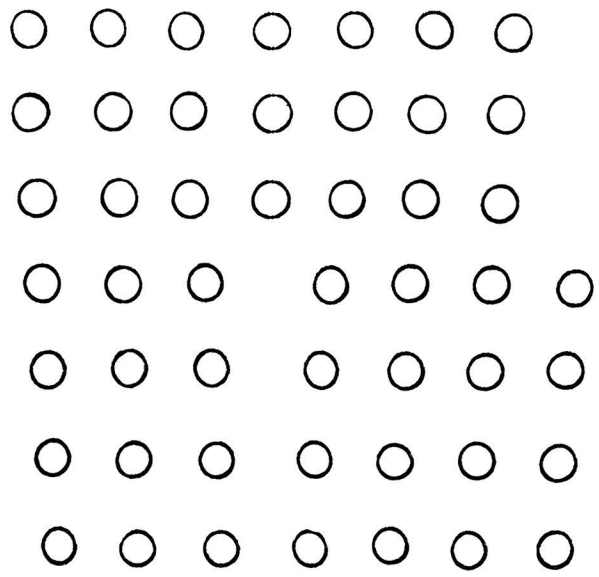

Fig. 3. Slipped crystal lattice.

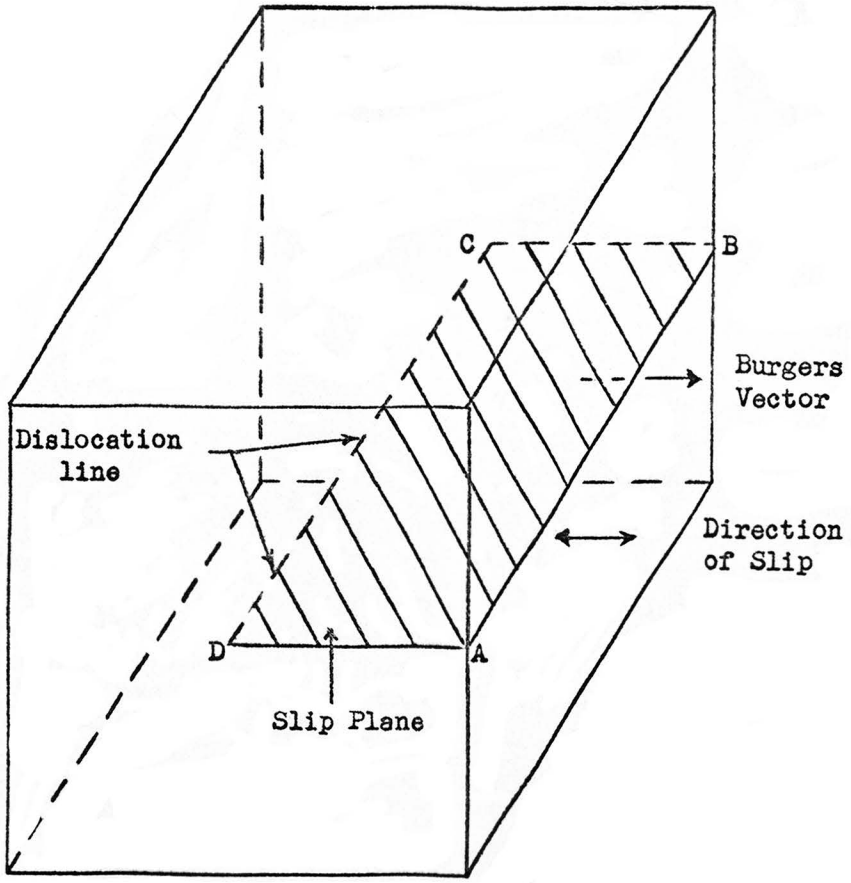

Fig. 4. Cubic crystal showing the relations of slip plane, dislocation line, Burgers vector and slip direction.

slip plane. The dislocation line lies along DC and consequently is in the slip plane. For an edge dislocation, the dislocation is perpendicular to the slip direction, which is, in turn, parallel to the Burgers vector.

As was mentioned in the INTRODUCTION, one theory which relies on the dislocation line accounting for the internal friction, is that of Granato and Lücke (2). Their model consists of a dislocation line having a total length L_n, referred to as the network length. The network length, assumed to be the same for all dislocations, is subdivided into smaller lengths, L, by impurity atoms. These impurity atoms hold their respective points of the dislocation line in a fixed position, a process referred to as "pinning" the dislocation line. Other points of the dislocation line are free to move, with the exception of the end points of L_n, which are held fixed by the crystal network. A diagram of this model is shown in Figure 5A.

If one applies a stress varying sinusoidally, for example a sound wave, the dislocation line will behave as a vibrating string as shown in Figure 5A, B, and C. If the stress is large enough, the dislocation line will break away from the impurity atoms as shown in Figure 5D and E, eventually collapsing to the original form as shown in Figure 5A. This type of model gives rise to two effects which can account for the loss of energy and hence the internal friction. First, there will be a loss of energy due to the damping of the vibrating segments of the dislocation line. Second, if the stress is plotted versus the strain for the breakaway process shown in Figure 5D and 5E, a hystersis curve results. The area enclosed in this curve gives the loss of energy for this process. It is assumed then that the total logarithmic decrement

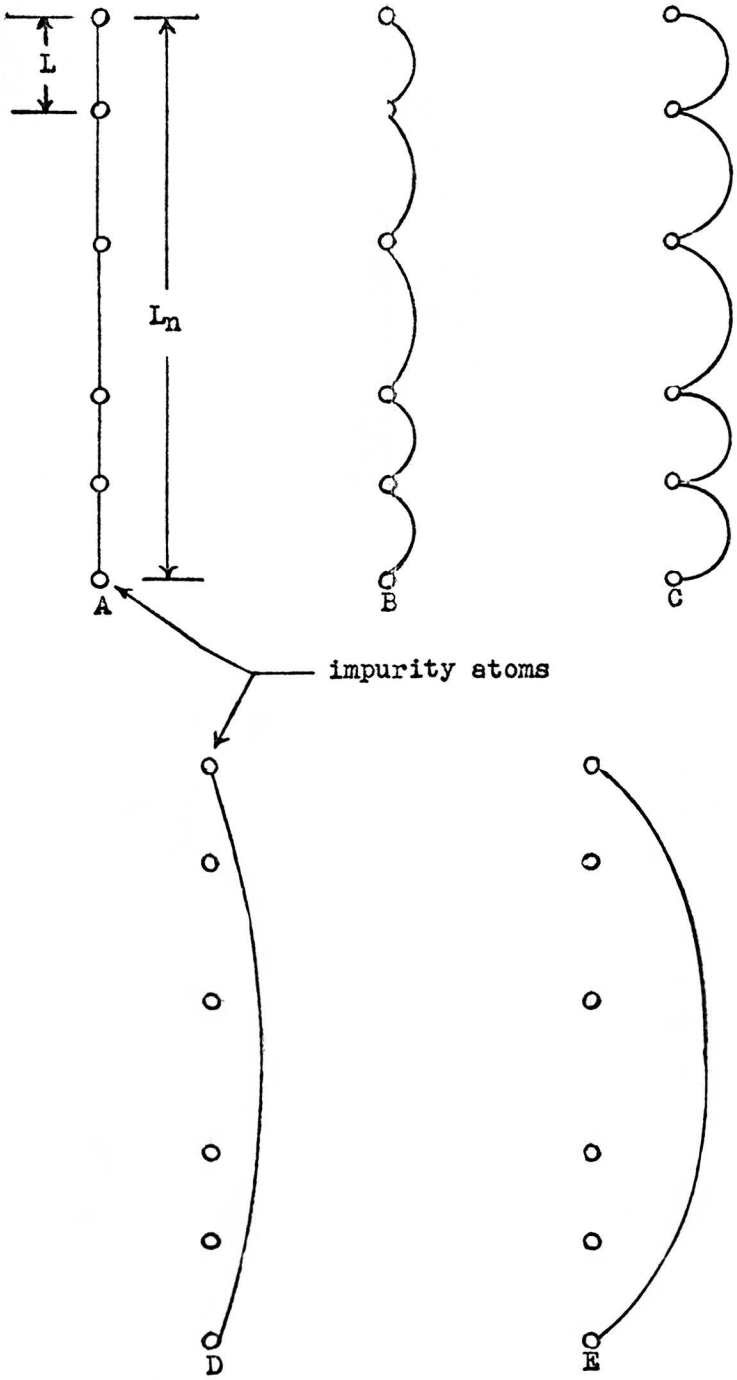

Fig. 5. Dislocation model under an applied stress.

can be expressed as a linear sum of the two terms, 1) the damping term, Δ_I, and 2) the hystersis loss, Δ_H.

Granato and Lücke show in their derivation of Δ_I and Δ_H that Δ_I is independent of the strain amplitude and dependent on the frequency, while Δ_H is independent of the frequency and dependent on the strain amplitude. Here, Δ_I is of primary interest.

The dependence of Δ_I on the frequency was approached by Granato and Lücke (2) by two different methods. First, they assumed that the distance between impurity atoms was a constant value L. This leads to

$$\Delta_I = \frac{\Delta_o \Lambda L^2 \Omega}{D\left[(1 - \Omega^2)^2 + \Omega^2/D^2\right]} \tag{2.3}$$

where Λ is the dislocation density, $\Omega = \omega/\omega_o$, where ω is the applied frequency and ω_o is the resonant frequency of the dislocation line, and $\Delta_o = 8Ga^2/(C\pi^3)$. Here G is the shear modulus, a is the lattice spacing, C is the tension per unit length due to the bowed out dislocation line, and $D = \omega_o A/B$. A is the mass per unit length of the dislocation line, and B is the damping constant per unit length.

A plot of the normalized decrement, $\Delta_I/(\Delta_o \Lambda L^2)$, versus the normalized frequency, ω/ω_o, is shown in Figure 6. There are seen to be two families of curves, one for large damping, $D \ll 1$, and one for small damping, $D \gg 1$. The dependence of the decrement on the frequency can be seen easily from the graph, with the maximum occurring at $\omega = \omega_o$ for small damping and at $\omega = \omega_o^2 A/B$ for large damping.

The second method was to assume that the distance between impurity atoms is not a constant value L, but obeys a distribution function such that the number of loops having a length between L and L + dL

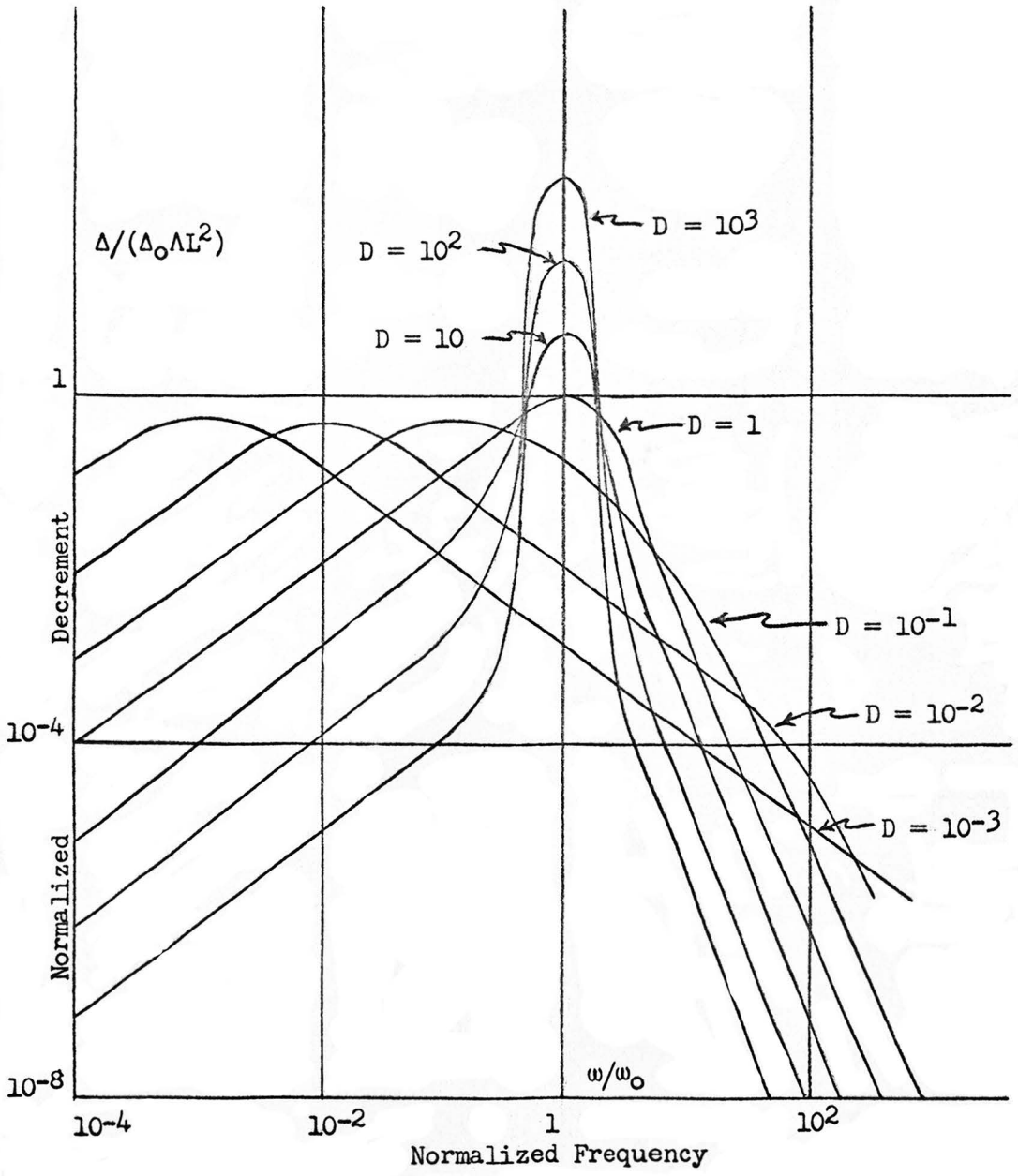

Fig. 6. The frequency dependence of the decrement for various values of the damping constant, assuming the distance between impurity atoms is constant.

is given by

$$N(L)\,dL = \frac{\Lambda \exp(-L/L_c)}{L_c^2}\,dL \qquad (2.4)$$

where L_c is the average loop length between impurity atoms. The dependence of the amplitude independent decrement as a function of frequency was calculated and plotted by Granato and Lücke (2) for this distribution of loop lengths. The results are shown in Figure 7 where it can be seen that the large maximum that occurred at resonance for small damping has been greatly reduced while the maximum at which the large damping occurred has been shifted to smaller frequencies.

If the frequency of the applied stress is much smaller than the resonant frequency, Granato and Lücke (2) show that the amplitude independent decrement depends approximately linearly on the frequency as given by

$$\Delta_I \approx \frac{\Omega \Delta_o \Lambda (L_c)^4 (5!) B\omega}{\pi^2 C} \qquad (2.5)$$

where Ω is a factor which depends on the orientation of the crystal.

Calculations were made to determine the shape of the theoretical curve for the normalized decrement versus the normalized frequency for a sample of aluminum. The value of D for aluminum was calculated to be 10^{-1} from the equation $D = \omega_o A/B$. A in this equation is given by Granato and Lücke (2) as $A = \pi \rho a^2$, where ρ is the density of the metal and a is the lattice spacing. The values used to calculate D, along with the source from which the numerical values were taken, are given in Table I.

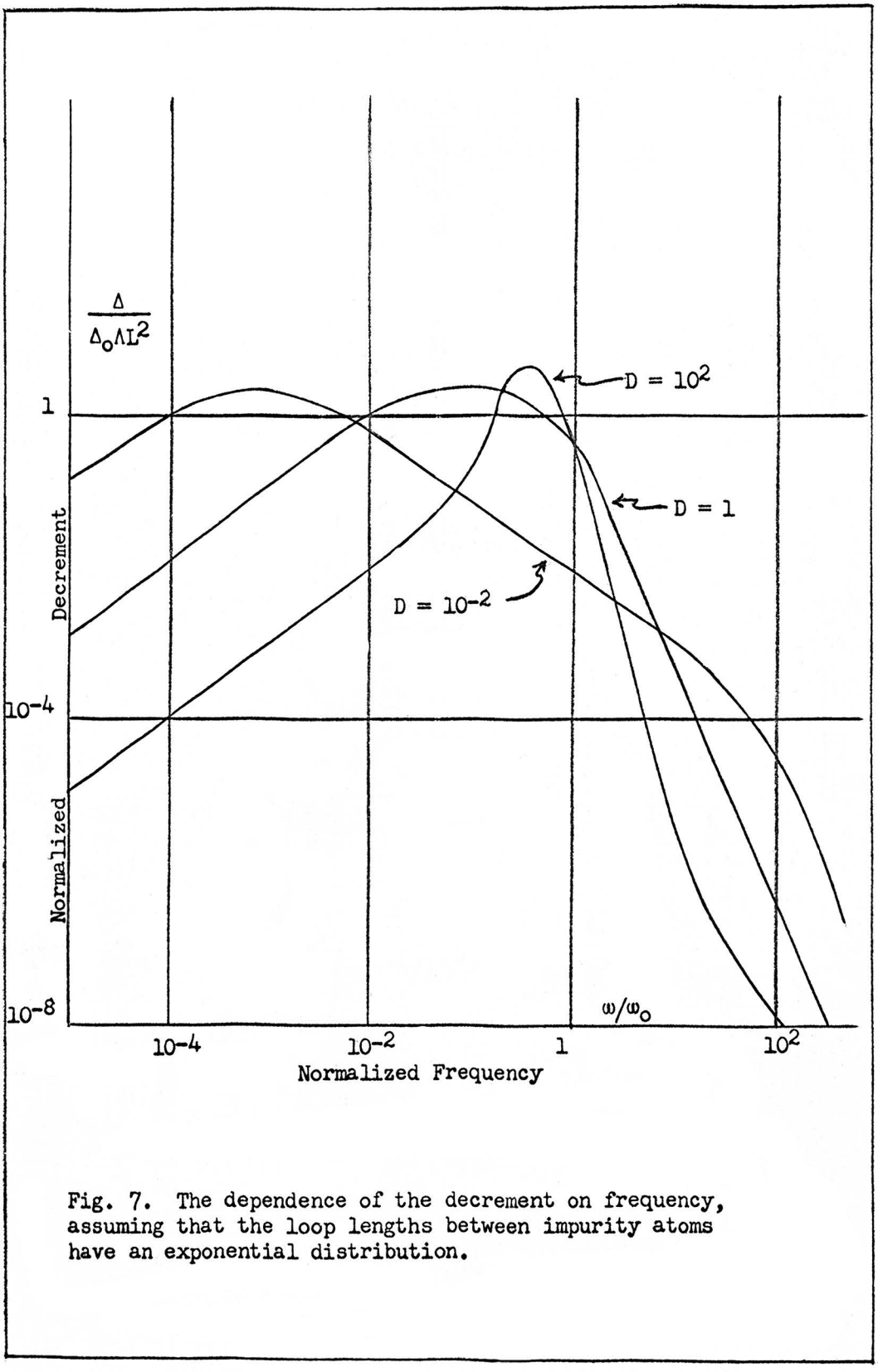

Fig. 7. The dependence of the decrement on frequency, assuming that the loop lengths between impurity atoms have an exponential distribution.

Symbol	Definition	Numerical Value	Source of Numerical Value
ρ	Density	2.7 gm/cc	Handbook of Physics and Chemistry
a	Lattice Spacing	4.04×10^{-8} cm	Handbook of Physics and Chemistry
$A = \pi\rho a^2$	Mass per unit length of the dislocation line	138 x 10-16 gm/cm	Formula from Granato and Lücke (2)
ω_o	Resonant frequency of the dislocation line	875 MC/sec	Granato and Lücke (1)
B	Damping constant per unit length of the dislocation line	1.1×10^{-5} gm/(sec cm) (average value)	Granato and Lücke (1)

Table I. Values used to calculate $D = \omega_o A/B$ for aluminum.

The maximum damping in aluminum is calculated to occur at 66 megacycles per second (1). With this information, the value of D given above and the curves of Figure 7 as a guide, the normalized decrement versus the normalized frequency for aluminum was obtained and is shown in Figure 8.

A frequency range of 1 to 16 megacycles per second, corresponding to ω/ω_o between 1.13×10^{-3} and 1.8×10^{-2} is indicated on Figure 8. It can be seen that, theoretically, one would expect a linear dependence on the frequency for the amplitude independent internal friction at the low end of the frequency range. As the 16 megacycle point is approached, the curve begins to reach its maximum value and the linear dependence no longer holds.

Of course, it must be remembered that the D curve chosen depends strongly on the value of B, which is known only approximately. A smaller B would indicate a strict linear dependence on frequency by making D larger and increasing the position of the maximum decrement for large damping. A larger value of B would decrease the value of D and decrease the position of ω_{max} putting the maximum of the decrement in the frequency range from one to sixteen megacycles per second.

In an article by Alers and Thompson (8), B for copper is shown to vary linearly with temperature, ranging from 0 to 7.5×10^{-4} gm/(sec cm) for a temperature range of 0^o to 300^o K. Another calculation of B by Alers and Thompson (8), made from their frequency dependent data, indicated a value of 1×10^{-4} gm/(sec cm) at room temperature. They state that the reasons for the differences between the values of B for the two calculations is unknown. Since the work done here was at room temperature, it was concluded that the value of

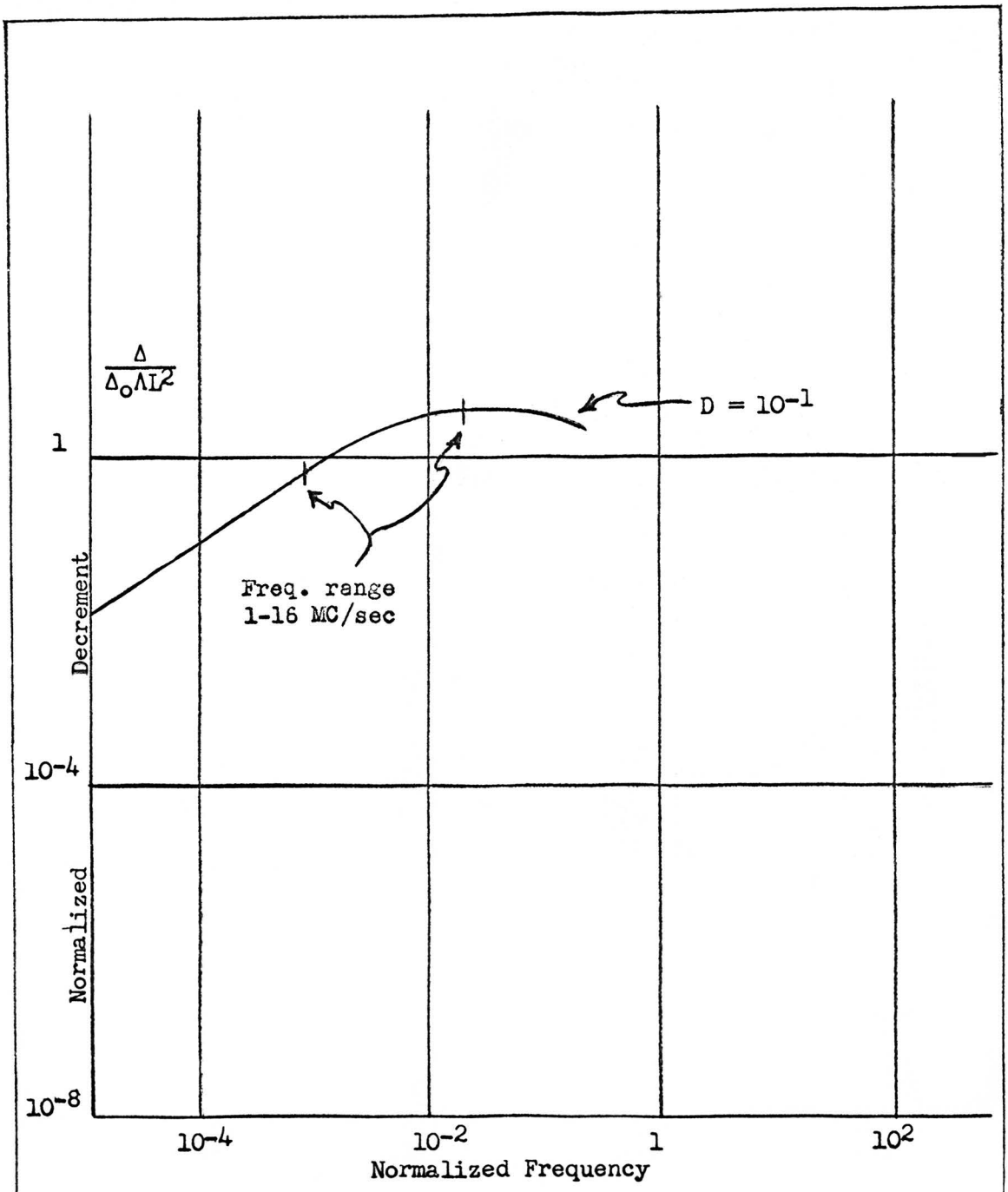

Fig. 8. The dependence of the decrement on frequency for aluminum, assuming that the loop lengths between impurity atoms have an exponential distribution

B chosen for aluminum to make a theoretical calculation was at least of the proper order of magnitude.

In the theory proposed by Granato and Lücke (2), it is noted that no mention of a dependence on temperature is made for the internal friction. As was explained above, Alers and Thompson (8) find a temperature dependence through the damping term B. Besides this temperature dependence, it was noted by Alers and Thompson (8) that the measurements of the decrement and modulus change, $\Delta G/G$, where G is the shear modulus, versus temperature, are different for kilocycle and megacycle studies. Alers and Thompson (8) support Wilks (9) in the idea of a thermal relaxation process accounting for the above differences. According to Wilks (9), there will be some depinning of the dislocation line from impurity atoms which will occur in a mean time, t, related to the temperature T by

$$t = A \exp(Q/kT) \tag{2.6}$$

where k is Boltzman's constant, A is a constant, and Q is the activation energy. If the period of the applied stress is of the order of the mean relaxation time t, depinning will occur. This has the effect of increasing the average loop length and hence affecting the value of the decrement and the modulus change, since the decrement depends on the fourth power of the loop length and the modulus change depends on the square of the loop length.

Alers and Thompson (8) and Wilks (9) point out that the difference between the decrement and the change of modulus depends on the frequency. The relaxation time seems to be of the order of magnitude of the periods of frequencies in the kilocycle range. Frequencies in the

megacycle range appear to have periods too short compared to the relaxation time to account for any increase in loop length by depinning. For this reason, Alers and Thompson (8) point out that there is some doubt about the validity of the Granato and Lücke theory in the kilocycle range.

A plot by Alers and Thompson (8) of the frequency versus the amplitude independent decrement, for a well annealed copper crystal between 10 and 80 megacycles per second, shows good agreement with the theory of Granato and Lücke (2). The only difference is in the position of the maximum. This might be expected as this position depends strongly on the value of B and, hence, the temperature.

As the relaxation time depends on the temperature, a study was made of the data given by Alers and Thompson (8) and the samples given by Wilks (9). Indications were that at room temperature and for frequencies in the megacycle range, this thermal relaxation process would not affect any experimental work done.

In their review article, Niblett and Wilks (3) state that experimental verification of the frequency dependence of the amplitude independent decrement is not at all conclusive. Hiki (10) measured the internal friction of single crystals of lead at a fundamental frequency of 64 kilocycles per second and at a third harmonic and found that the amplitude independent internal friction was proportional to the frequency in the temperature range of 140° to 220° K. Hikata and Truell (11) found that the amplitude independent internal friction was proportional to the frequency at five and ten megacycles. Working at a fundamental frequency of 39 kilocycles and a second harmonic of 78 kilocycles per second on a single crystal of copper, Norwick (12) reported that even though his results were scattered, the amplitude

independent internal friction appeared to be independent of the frequency. Experimental data given by Takahoshi (13) on polycrystalline copper indicated no frequency dependence of the amplitude independent internal friction between one and ten kilocycles per second. Bordoni's (14) work on polycrystalline copper found little change in the amplitude independent internal friction between the frequency range of 1.8 kilocycles per second to 6.5 megacycles per second. Measurements by Granato and Truell (7) on germanium single crystals displayed the linear dependence on frequency of the amplitude independent friction, but as Niblett and Wilks (3) point out, germanium is a semiconductor; consequently these results may not be typical of metals.

It can be concluded that the general results are inconsistent regarding the frequency dependence of the amplitude independent internal friction. The kilocycle measurements as performed by Hiki (10) and Norwick (12) were done by use of the composite oscillator. The main disadvantage of this method is that only harmonics of the fundamental frequency can be used. When a harmonic is employed, the positions of the maximum stress of the standing waves shifts relative to the positions of the maximum stress for the fundamental frequency and other harmonics. As the dislocation density may not be uniform throughout the sample, experiments of this type may not yield the true frequency dependence.

The pulse technique, which relies on a burst of ultrasonic waves, and not on a standing wave pattern, has a definite advantage in measurements designed to test the frequency dependence of the amplitude independent internal friction. Here, the pulse width must be much

greater than the period of the ultrasonic wave to insure a sufficiently narrow Fourier spectrum.

Of the references mentioned above on the experimental results regarding the frequency dependence of the amplitude independent internal friction, only those performed by Granato and Truell (7), Alers and Thompson (8) and by Truell and Hikata (11) made use of the pulse technique.

III. EXPERIMENTAL TECHNIQUES

The pulse echo technique, as described by Roderick and Truell (15), can be used to measure the internal friction of a metal sample.

In using this method, a piezoelectric crystal is cemented to the sample surface with a metal electrode placed on top of the piezoelectric crystal. When a pulse from the ultrasonic generator is applied to the electrode, an oscillating electric field is established in the piezoelectric crystal, causing it to vibrate mechanically. These vibrations are transmitted to the sample as waves which travel the length of the specimen, are reflected at the free end, and travel back to the piezoelectric crystal. Here the mechanical vibrations are transformed into an electrical pulse by the inverse piezoelectric effect. This pulse is amplified electronically and displayed on an oscilloscope. The wave, which was reflected at the transducer, travels down and back the length of the specimen, where again an electrical impulse is amplified and displayed on the oscilloscope. This process continues until the wave is completely attenuated and a new electrical pulse from the generator is applied to the electrode.

If the complete set of reflected pulses or echoes is displayed on the screen of the oscilloscope, the results should exhibit an exponential decay of amplitude, as shown by Granato and Truell (15). The envelope of the pulses displayed can be expressed as

$$E = E_0 \exp(-\alpha v t) \qquad (3.1)$$

where E_0 is the electrical amplitude of the first echo. This equation is true provided the reflection coefficient is unity on both faces of the sample. Here, v, is the velocity of the wave in the medium, t is

the time the wave traveled in the specimen, and α is the attenuation coefficient. Taking $\log_{10}$ of both sides of this equation yields the following expression.

$$20 \log_{10}(E_o/E) = 8.68\alpha vt \qquad (3.2)$$

$20 \log_{10}(E_o/E)$ gives the attenuation of E in decibels with respect to E_o. Hence the attenuation can be plotted versus the time t of travel to obtain $8.68\alpha v$, the slope of this line. As the logarithmic decrement, Δ, is related to the attenuation coefficient, α, by

$$\Delta = \alpha v/f \qquad (3.3)$$

the logarithmic decrement can be calculated. Here f is the frequency of the wave.

The procedure, then, consists of applying a pulse of ultrasonic waves of the desired frequency to the sample, photographing the exponential decay on the oscilloscope, finding α from the graph of attenuation versus time, and calculating the logarithmic decrement from the above relation. This procedure is repeated for as many frequencies as desired.

As the frequency range of interest here was from 1 to 16 megacycles per second, X cut quartz crystals, having fundamental frequencies of 1.0, 1.2, 1.5, 1.8, 2.2, 2.7, 3.3, and 4.0 megacycles per second were purchased from a commercial supplier. The 1.0 and 1.2 megacycles per second crystals were one inch in diameter while the rest were 1/2 inch in diameter. Their surfaces were polished to allow higher harmonics to be generated. Only odd harmonics were generated, as even harmonics cancel in the quartz crystal (14).

A block diagram of the equipment is shown in Figure 9. As the amplifier used here began to lose gain for frequencies above 1 megacycle per second, it was used as an intermediate frequency amplifier in a heterodyne detection system. Here the frequency of the incoming pulse is mixed with that of a local oscillator to produce a difference frequency in a range to utilize the gain of the amplifier. For example, if a 16 megacycle pulse were used, a local 15 megacycle oscillation mixed with the 16 megacycle pulse would produce a 1 megacycle pulsed oscillation. This allows the maximum gain of the amplifier to be employed.

As can be seen from the block diagram, an electrode rests on the piezoelectric transducer. The transducer, in turn, was fastened to the sample by use of a Dow Corning silicone compound having a viscousity of 2,000,000 centistokes.

There are two basic techniques which can be used when employing the pulse method. In one, the specimen to be tested has a diameter large compared to that of the piezoelectric crystal. In the other, the piezoelectric crystal diameter is of the same size as that of the sample. In the first method, one assumes that the specimen appears as an unbounded medium, so that the boundaries have little effect on the attenuation of the ultrasonic wave. This method has been analyzed both experimentally and theoretically by Siki, Truell and Granato (17). The decay pattern is found to be non-exponential due to beam spreading and diffraction affects.

The second method, referred to as the cylindrical wave guide technique, ideally should have no losses other than those due to the intrinsic properties of the sample tested. Redwood (18) shows both

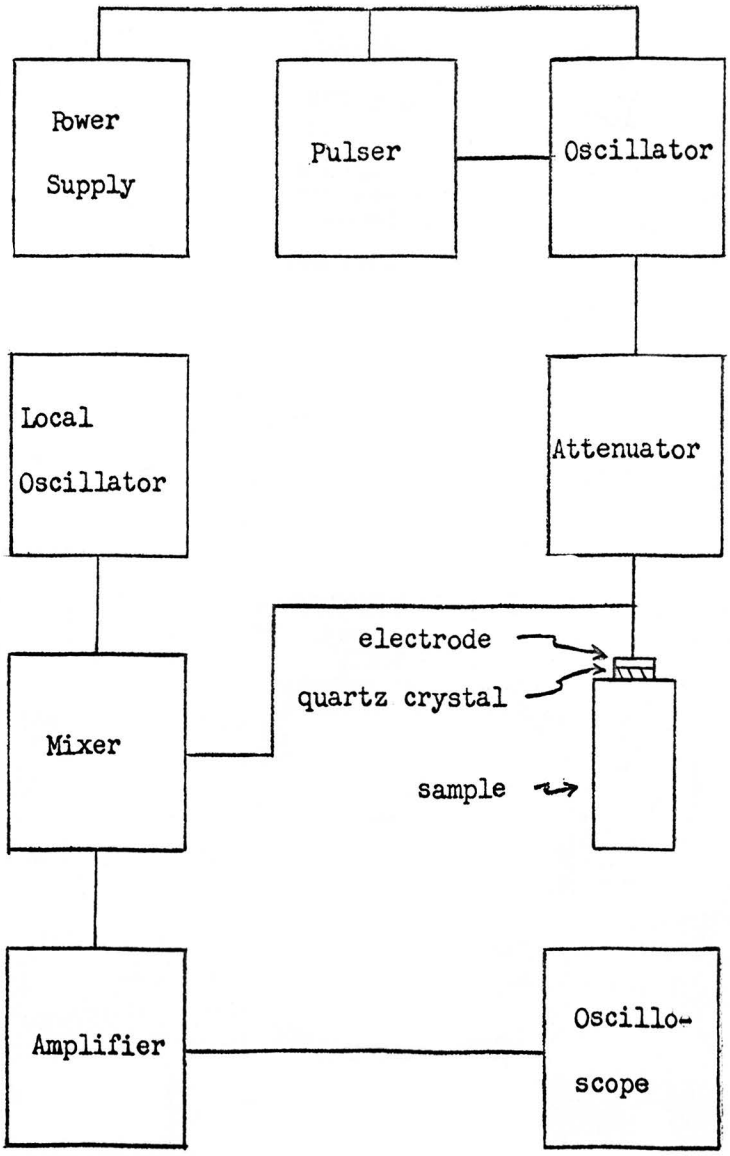

Fig. 9. Block diagram of experimental arrangement.

analytically and experimentally, that this method yields a decay pattern that is non-exponential due to two reasons. First, the different modes excited in the sample form an interference pattern. Secondly, the conversion of longitudinal waves to transverse waves and vice versa, at the side boundaries, produce trailing pulses, due to the different velocities of transverse and longitudinal waves, which remove energy from the main pulse.

The cylindrical wave guide technique has the advantage that the sample does not have to have dimensions which are so large as to be impractical, in contrast with the first method. This technique was chosen for use here.

The sample to be tested was a single crystal of aluminum, purchased from Semi Elements Inc., Saxonburg, Pennsylvania. The single crystal, 99.995% pure, was 4.0 inches long and had a diameter, uniform to within one ten thousandth of an inch, of $1.00 \pm .01$ inches. The end faces were flat and parallel to within .001 inch. To obtain the maximum effect of the dislocations present, the cylinder axis was oriented to within 1° of the 110 axis, the slip direction for aluminum.

For the experiment, the single crystal was held secure in a holder shown in Figure 10. The holder consisted of a block of aluminum at the center of which were turned two concentric circular holes. This formed a lip on which the single crystal could rest, and allowed the sample to have an air boundary over the greater portion of its end face. The base of the holder was surrounded on three sides with sheet aluminum to which two coaxial connectors were fastened. One of these coaxial connectors served to bring the ultrasonic pulse to the sample, and the other to transmit the echoes to the amplifier either directly

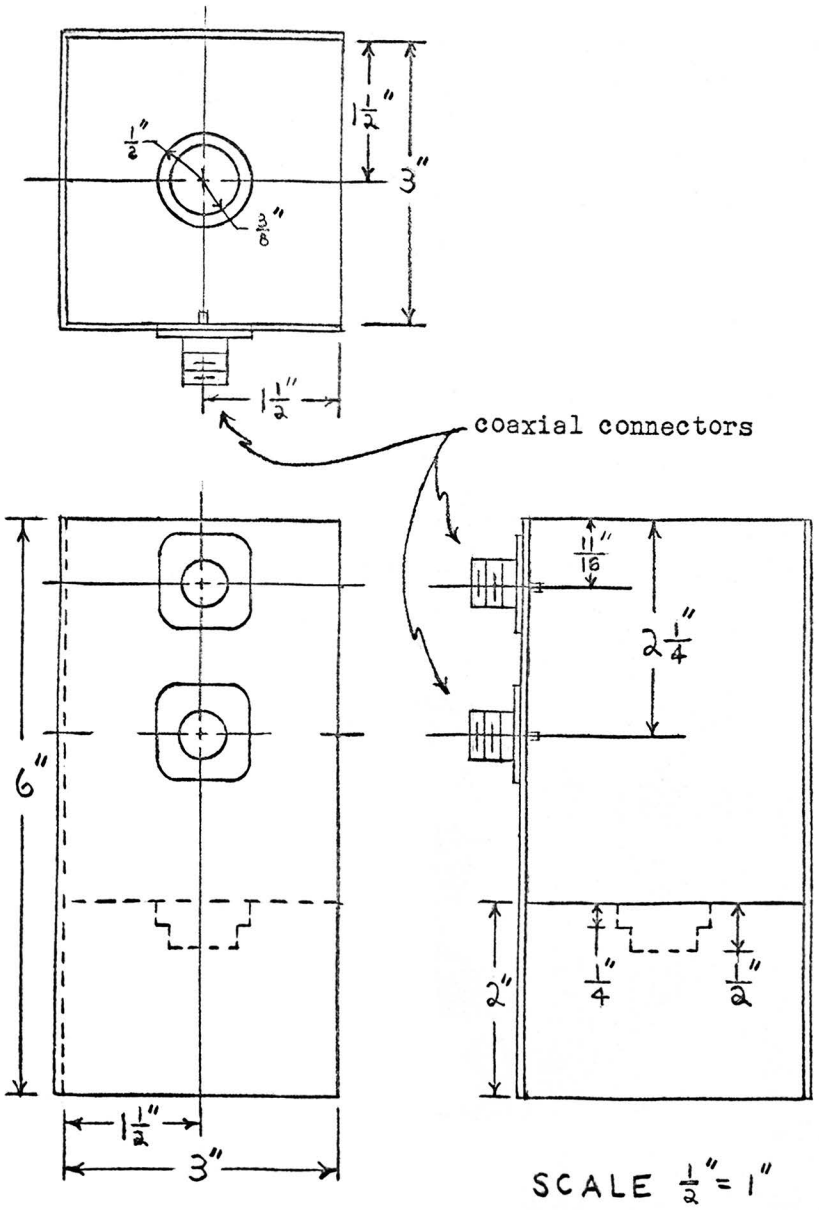

Fig. 10. Holder for the single crystal of aluminum.

or through the heterodyne mixer. The ground terminal of the coaxial connector was connected directly to the holder. As the sample made contact with the holder, the sample became the second electrode for the piezoelectric crystal. The electrode which delivered the signal from the generator to the piezoelectric crystal was placed on top of the crystal and was constructed of bronze, 1/8 inch thick and 1/2 inch in diameter.

Mason (19) illustrates a typical result of the cylindrical wave guide technique observed on a one inch diameter crystal of aluminum at a frequency of 5 megacycles per second. This is shown in Figure 11. The effect of the interference modes can be minimized by the use of an electrode which has a slightly smaller radius than that of the sample tested. This arrangement gives echoes that decay exponentially, with the trailing pulses being small enough as to contain only a small amount of the total energy of the pulse. Good experimental data is obtainable for frequencies above five megacycles per second on a one inch diameter aluminum crystal. For this reason, the electrode was chosen to have a diameter of 1/2 inch, while the diameter of the single crystal of aluminum was one inch.

One other criterion was followed in chosing the diameter of the sample. Mason (20) states that experimental evidence indicates that the pulsed longitudinal ultrasonic wave will be distorted to such a degree that trailing pulses will be produced which become negligible compared to the main pulse only when the diameter of the sample is twenty or more times the wave length. A one inch diameter crystal of aluminum is found to obey this criterion for frequencies above five megacycles per second.

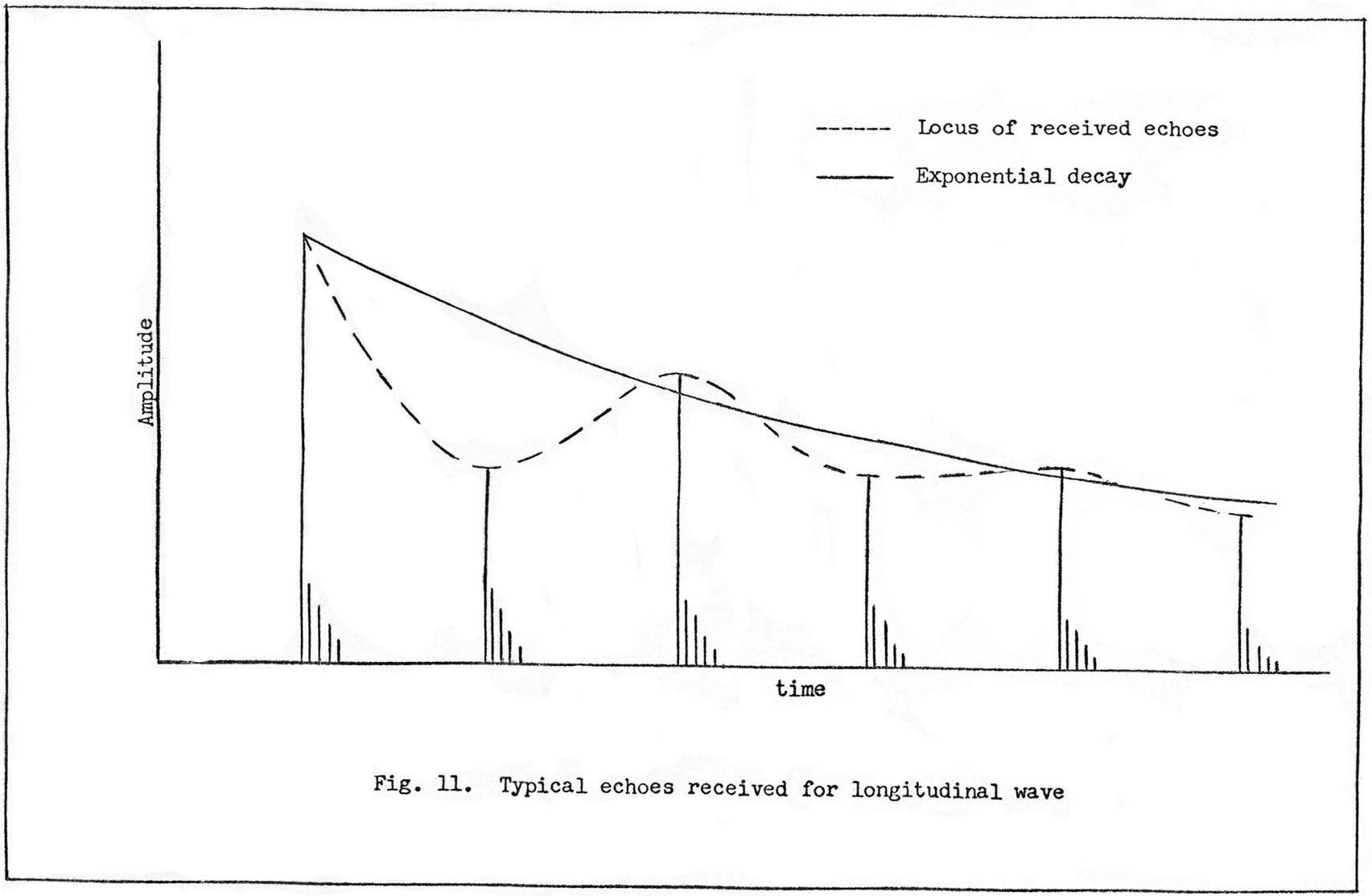

Fig. 11. Typical echoes received for longitudinal wave

The only other losses considered here are: 1) loss due to grain boundary scattering, 2) loss due to the end faces being non-parallel, 3) reflection losses at the free end of the sample, and 4) reflection and absorption losses in the medium bonding the quartz piezoelectric crystal to the sample.

The loss due to scattering is dependent on the wave length and hence the frequency of the ultrasonic wave. As a single crystal was used here and there were no grain boundaries present, a loss of this type was not expected.

Granato and Truell (7) point out that if the faces of the sample being tested are not parallel, the wave front of the plane ultrasonic wave will become distorted, causing a loss which is dependent on the wave length and hence the frequency. For this reason, the faces of the sample were made flat and parallel to within .001 inch.

Of the last two losses possible, Redwood and Lamb (21) state that the losses at the free end of the sample are small enough to be considered negligible. In this same article and in another by Redwood (18), a method is outlined to measure the losses due to the reflection and absorption of the ultrasonic wave at the medium bonding the piezoelectric crystal to the sample being tested. It is stated in both of these articles, that this loss may be as high as one decibel, but is usually of the order of a tenth of a decibel.

In an experiment which is concerned only with observing the frequency dependence of the amplitude independent decrement, an absolute measurement of the attenuation is not necessary as long as the loss for each frequency tested is the same. For this reason, the last two losses mentioned above are considered uniform for all

frequencies tested and as having no affect on the measurements. Those losses which are frequency dependent, as first pointed out, are assumed small enough not to affect the validity of any data.

If we consider only measurements for the strain amplitude independent decrement, it is necessary to know the order of magnitude of the strain developed. The equation (19) for the strain of the quartz crystal, S_1, due only to an applied electric field, E_x, reduces to

$$S_1 = d_{11} E_x \tag{3.4}$$

where d_{11} is -2.25×10^{-10} cm/volt. The maximum potential of the pulse from the apparatus constructed here was of the order of 1,000 volts peak to peak. For a field, E, of 1,000 volts/cm, the strain, S_1, is 2.25×10^{-7}. As this crystal vibrates against the single crystal of aluminum, the strain can be considered no larger than 10^{-7}. Niblett and Wilks (3) show graphically, that the strain amplitude dependent internal friction occurs for strains in excess of 10^{-6}, so that theoretically it appears that one could expect only the amplitude independent decrement to be that quantity measured with the use of a 1,000 volt pulse.

Experimentally, Alers and Thompson (8) state that in their work with copper, a voltage of .7 to 400 volts peak to peak was applied to a quartz transducer and the resulting attenuation was strain amplitude independent.

For this reason and for fear of fracturing the quartz crystal by use of a pulse having a thousand volts peak to peak, an attenuator was placed in the circuit to reduce the peak to peak voltage of the pulse to below 400 volts. Hence with the use of these low voltages, it can

be safely assumed that any data obtained can be for strain amplitude independent conditions.

IV. EQUIPMENT

The block diagram of the electronic equipment, consisting of a power supply, pulser, oscillator, attenuator, mixer, local oscillator and amplifier is shown in Figure 9. The amplifier was constructed by Koelling (22).

The pulser and oscillator were adapted from a design by Skudrzyk (23). The equipment can be broken down into four main parts. These are the thyratron pulse circuit, the multivibrator, the cathode follower and the oscillator, shown in Figures 12, 13, 14 and 15 respectively. The values of the components are given in Table II and III. The 480 volt plate supply for the pulser and the oscillator was obtained from a dual regulated power supply, a product of Kepco Labs of Flushing, New York. This supply has a range of 0-600 volts D. C. and 0-250 milliamps.

The pulser, which forms the first three of the above mentioned stages, was built according to the specifications of Skudrzyk (23). The same oscillator was used, but various combinations of capacitors and inductors were used to give the desired frequency range.

The pulser is intended to give a repetition rate ranging from 1 pulse every ten seconds, to one pulse every 40 microseconds, with a range of pulse widths from 1/3 of a microsecond to 100 milliseconds. It was found experimentally, that the repetition rate range was from 1 pulse every 5 seconds to one pulse every 15 milliseconds, with a range of pulse widths of 4 microseconds to 10 milliseconds. It was assumed that the reason the characteristics are not as good as those established by Skudrzyk (23) is that long leads may have introduced

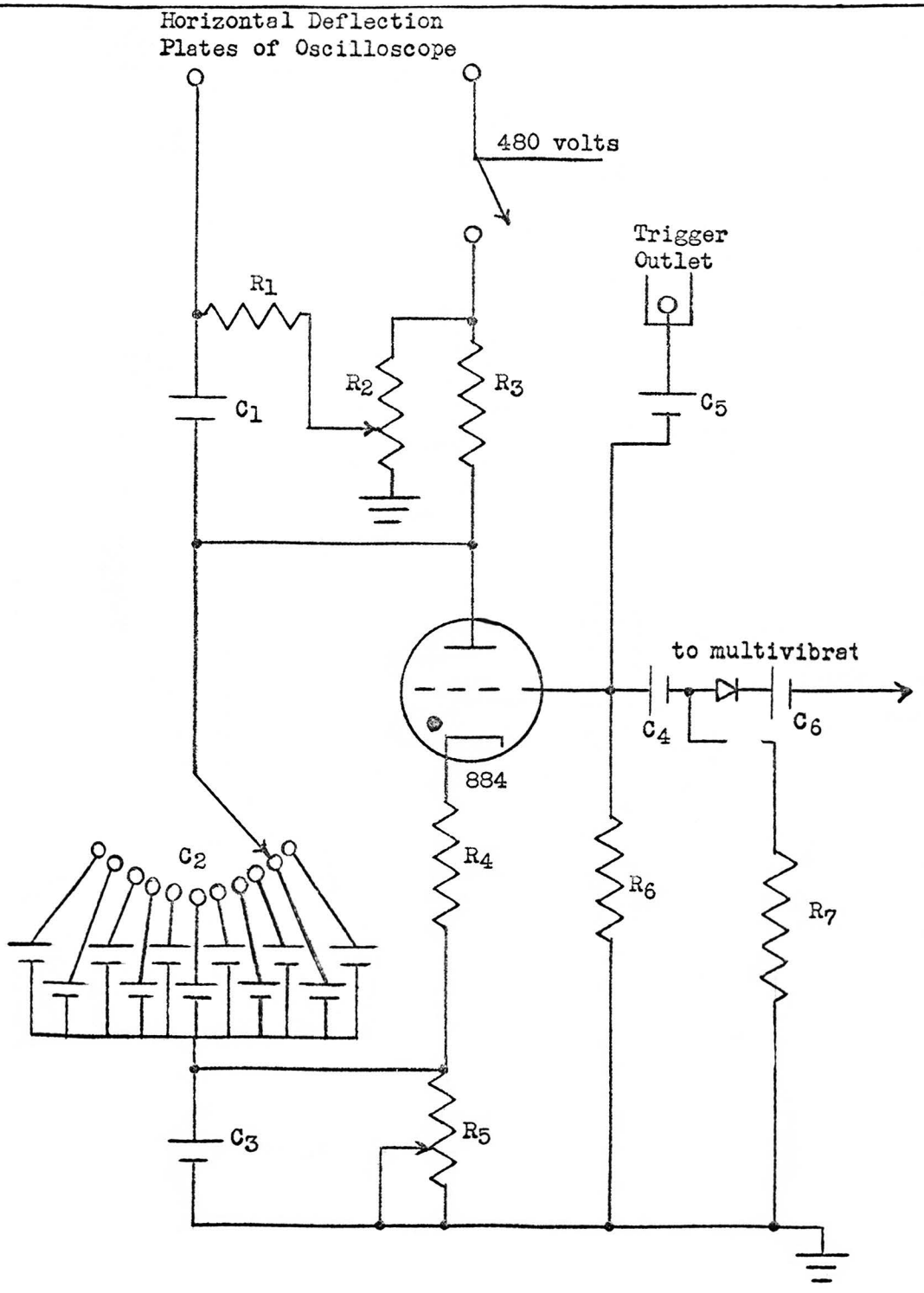

Fig. 12. Thyratron circuit.

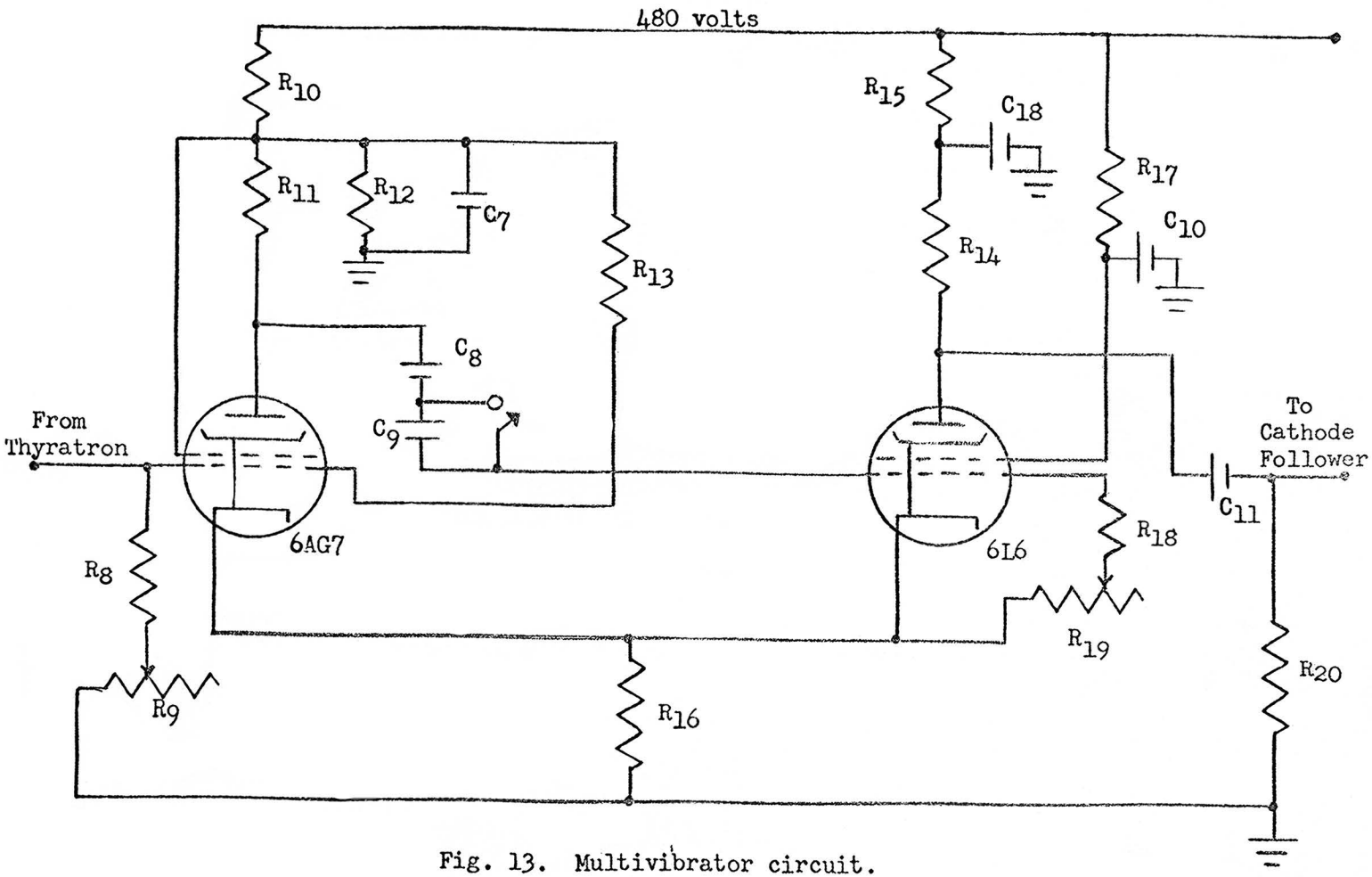

Fig. 13. Multivibrator circuit.

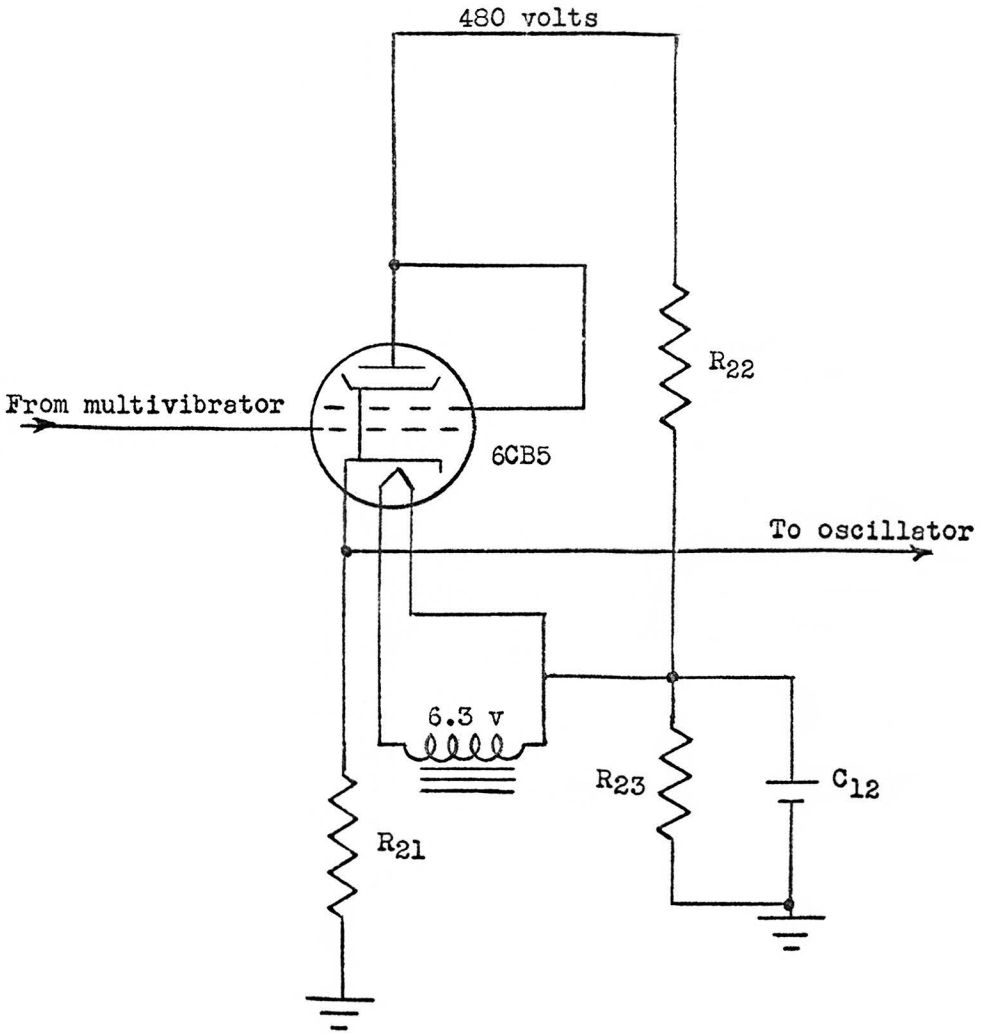

Fig. 14. Cathode follower.

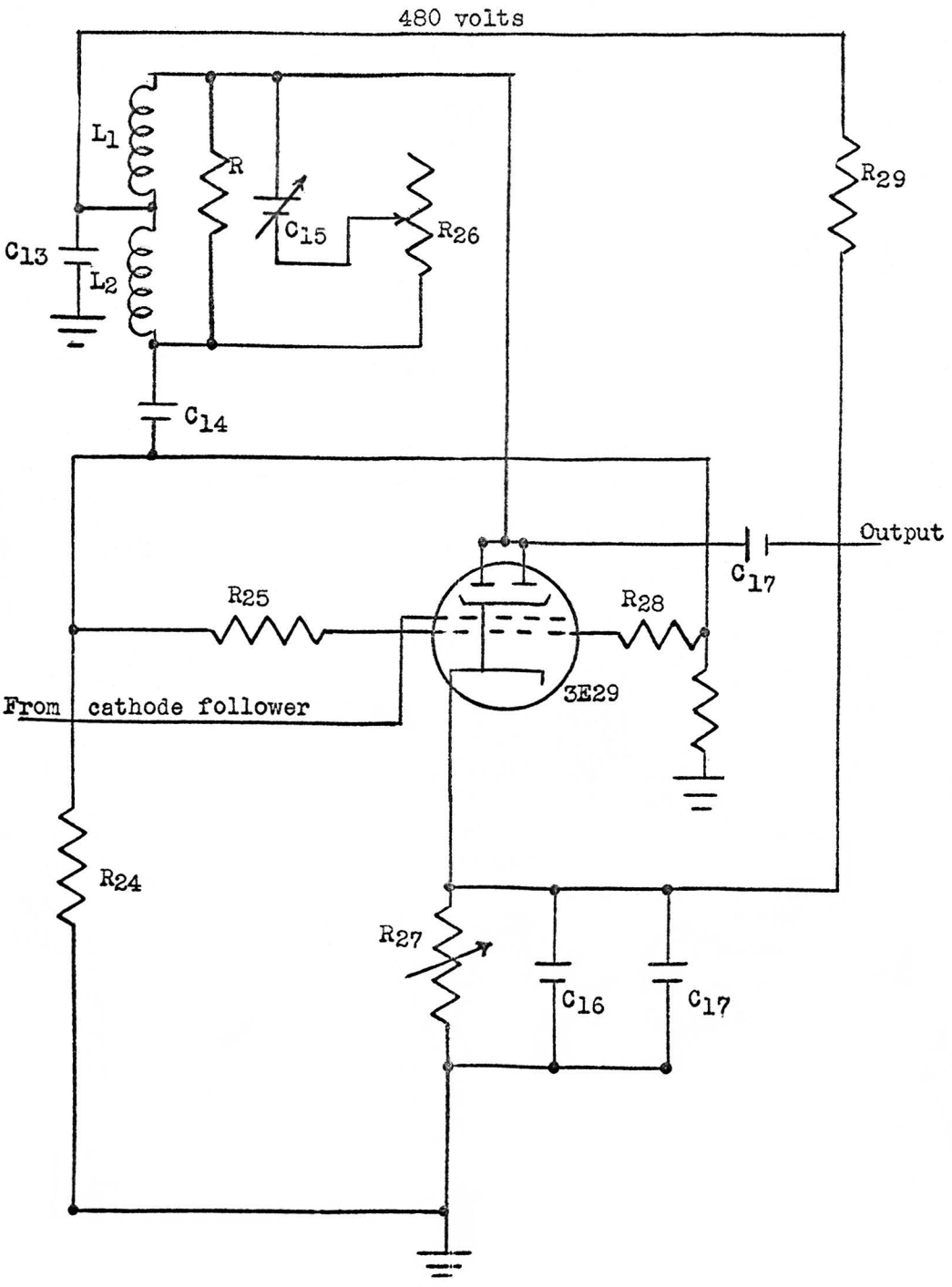

Fig. 15. Oscillator circuit.

R_1- 1 meg-ohm, 1/2 watt

R_2- 500 kilo-ohms, 2 watts

R_3- 400 kilo-ohms, 1/2 watt

R_4- 1 kilo-ohm, 1/2 watt

R_5- 100 kilo-ohms, 2 watts

R_6- 50 kilo-ohms, 1/2 watt

R_7- 10 kilo-ohms, 1/2 watt

R_8- 2 kilo-ohms, 1/2 watt

R_9- 5 kilo-ohms, 2 watts

R_{10}- 50 kilo-ohms, 5 watts

R_{11}- 3 kilo-ohms, 5 watts

R_{12}- 50 kilo-ohms, 1/2 watt

R_{13}- 180 kilo-ohms, 1/2 watt

R_{14}- 5 kilo-ohms, 20 watts

R_{15}- 500 ohms, 2 watts

R_{16}- 180 ohms, 1 watt

R_{17}- 22.5 kilo-ohms, 10 watts

R_{18}- 200 ohms, 1/2 watt

R_{19}- 1 meg-ohm, 2 watts

R_{20}- 180 kilo-ohms, 1/2 watt

R_{21}- 3 kilo-ohms, 10 watts

R_{22}- 500 kilo-ohms, 1/2 watt

R_{23}- 400 kilo-ohms, 1/2 watt

R_{24}- 30 kilo-ohms, 1/2 watt

R_{25}- 50 ohms, 1/2 watt

R_{26}- 5 kilo-ohms, 20 watts

R_{27}- 1 kilo-ohms, 20 watts

R_{28}- 50 ohms, 1/2 watt

R_{29}- 75 kilo-ohms, 5 watts

R- 5 kilo-ohms, 1/2 watt

Table II. Values of resistors for generator.

C_1- 0.1 mf, 600 v

C_2- 25, 50, 100, 200, 400 mmf;
0.001, 0.003, 0.01, 0.05,
0.2, 0.5, 2 mf, 600 v

C_3- 50 mf, 50 v

C_4- 50 mmf, 1,000 v

C_5- 10 mmf, 1,000 v

C_6- 50 mmf, 1,000 v

C_7- 8 mf, 250 v

C_8- 0.01 mf, 1,000 v

C_9- 100 mmf, 500 v

C_{10}- 8 mf, 450 v

C_{11}- 1 mf, 450 v

C_{12}- 0.2 mf, 250 v

C_{13}- 0.5 mf, 600 v

C_{14}- dependent on frequency

C_{15}- 66-1,700 mmf and 20-135 mmf

C_{16}- 0.02 mf, 100 v

C_{17}- 100 mmf, 100 v

C_{18}- 0.2 mf, 600 v

L_1- according to frequency

L_2- according to frequency

Table III. Values of capacitors and inductors for generator.

added capacitance and inductances which change the operating characteristics of the circuit. As the results obtained were in a region of satisfactory working conditions, no time was spent on the redesign of the circuit.

In the thyratron circuit, as shown in Figure 12, C_1, R_1 and R_2 are used for a horizontal display of the input if this is desired. The basic function of the thyratron circuit is to determine the pulse repetition rate. Essentially, a current charges one of the capacitors in the bank of capacitors labeled C_2. The charging process continues, the rate of charging determined by R_3C_2, until the plate potential of the thyratron becomes large enough to allow the tube to fire. This charging time then determines the time between pulses and hence the repetition rate. The bank of capacitors C_2, along with the cathode biasing resistor R_5, allows control over the repetition rate. As R_5 controls the potential of the cathode, an adjustment on R_5 will determine the potential at which the plate will fire by changing the relative plate to cathode potential. The rest of the circuit consists of biasing resistors, differentiating circuits and a diode which forms the pulse fed into the multivibrator.

The operation of the cathode coupled multivibrator shown in Figure 13 can be outlined in the following steps. Let us consider that initially the 6L6 is conducting, while the 6AG7 is not. If a positive pulse is applied to the grid of the 6AG7 from the thyratron circuit, the result is to cause this tube to conduct. Since the capacitor C_8 or C_8 and C_9 in series cannot discharge instantaneously, the decrease in the plate potential of the 6AG7 is seen by the grid of the 6L6 as a drop in potential. This is due to the grid current

through R_{18} and R_{19}. At the same time, the cathode potential of the 6L6 increases because of the conduction of the 6AG7 through R_{16}. This helps the grid to cathode potential to increase and shuts off the 6L6. As the capacitor discharge of C_8 or C_8 and C_9 in series becomes complete, the grid current through R_{18} and R_{19} goes to zero, allowing the grid potential of the 6L6 to rise to the cut off level and begin the 6L6 conducting. The increase of current through R_{16} is sufficient to raise the cathode potential of the 6AG7 so that the grid cathode voltage drops below the cut off level. As the 6AG7 ceases to conduct, the plate potential of the 6AG7 increases. Since C_8 or C_8 and C_9 in series cannot charge instantaneously, a grid current through R_{18} and R_{19} increases the grid potential of the 6L6 aiding the conduction. This in turn continues to increase the cathode potential of the 6AG7 due to the increase of current through R_{16}, driving the 6AG7 to a non-conducting state. Hence the original condition is re-established, the 6L6 conducting and the 6AG7 shut off. With another application of a positive pulse from the thyratron circuit, the above process is repeated.

Just as the repetition rate is developed in the thyratron circuit, the pulse width is controlled in the multivibrator circuit by the time interval the 6L6 is non-conducting. This time is the RC time constant given by R_{18} and R_{19} in series, and C_8 or C_8 and C_9 in series. Control over the pulse width lies in the variable resistor R_{19} and in a switch which determines whether C_8 is used singly or in series with C_9. A more complete description of multivibrators can be found in Ryder (24).

The rest of the multivibrator circuit consists of biasing resistors, and capacitors to maintain constant voltages. The circuit

consisting of R_{12}, C_7, R_{13}, R_8 and R_9 keeps a fairly constant potential on the grid of the 6AG7. It is found experimentally, that R_9 can be adjusted so that the multivibrator does not function. This is expected, since if the grid potential is made negative enough the positive pulse from the thyratron circuit is not large enough to begin the 6AG7 conducting.

The pulse from the multivibrator, taken off the plate of the 6L6, is fed to the grid of the 6CB5 in the cathode follower circuit. This increases the flow of plate current, thus increasing the cathode potential due to the biasing resistor R_{21}. As the pulse dies out, the cathode returns to its original potential, thus forming a pulse on the cathode of the 6CB5, which is fed to the oscillating circuit. The function of the cathode follower is to act as an impedance transformer, as the output impedance of the multivibrator is high compared to the input impedance of the oscillator. If a mismatch of impedances between the multivibrator and oscillator were allowed, there would be a considerable loss of power. As is shown in the schematic of the cathode follower in Figure 14, the heater is supplied with a 200 volt D. C. positive potential to keep the heater from arcing over and breaking down the heater insulation.

The pulse from the cathode follower turns the oscillator on and off which then produces the pulse of ultrasonic waves.

The main concern with the oscillator, as shown in Figure 15, was that of finding the proper capacitors and inductors in the tank circuit to give the desired frequency range. The rest of the oscillator consists of biasing resistors and capacitors to maintain constant voltages.

If attention is focused on the tank circuit, as shown specifically in Figure 16, Eastman (25) shows that the resulting frequency can be given as

$$f = \frac{1}{2\pi\sqrt{LC_{eq}}} \tag{4.1}$$

where L is the plate inductance and C_{eq} is the equivalent capacitance of the rest of the tank circuit. Examination of the tank circuit of Figure 16 shows that L_1 is the plate inductor or L in the above equation. The rest of the components, L_2, R, C_{15} and R_{26} have to be combined to form the equivalent capacitance, C_{eq}. This was done by examining the combination of the impedances of the above components. The resulting C_{eq} is given as

$$C_{eq} = \frac{(R + R_{26})^2 + 1/(4\pi^2 f^2 C_{15}^2)}{R^2/C_{15} - (2\pi f)^2 L_2\left[(R + R_{26})^2 + 1/(4\pi^2 f^2 C_{15}^2)\right]} \tag{4.2}$$

Substituting this value of C_{eq} into equation (4.1) and solving for f, we obtain

$$f = \frac{1}{2\pi(R + R_{26})}\left[\frac{R^2/C_{15} + (1/C_{15}^2)(L_2 - L_1)}{L_2 + L_1}\right]^{\frac{1}{2}} \tag{4.3}$$

Given any inductor or capacitor, this equation allows the corresponding frequency to be calculated.

The oscillator was constructed using two variable capacitors, having ranges from 66 picofarads to 1700 picofarads, (labeled large capacitor) and 20 picofarads to 135 picofarads (labeled small capacitor) for C_{15}. A switch in the circuit gave the experimenter a

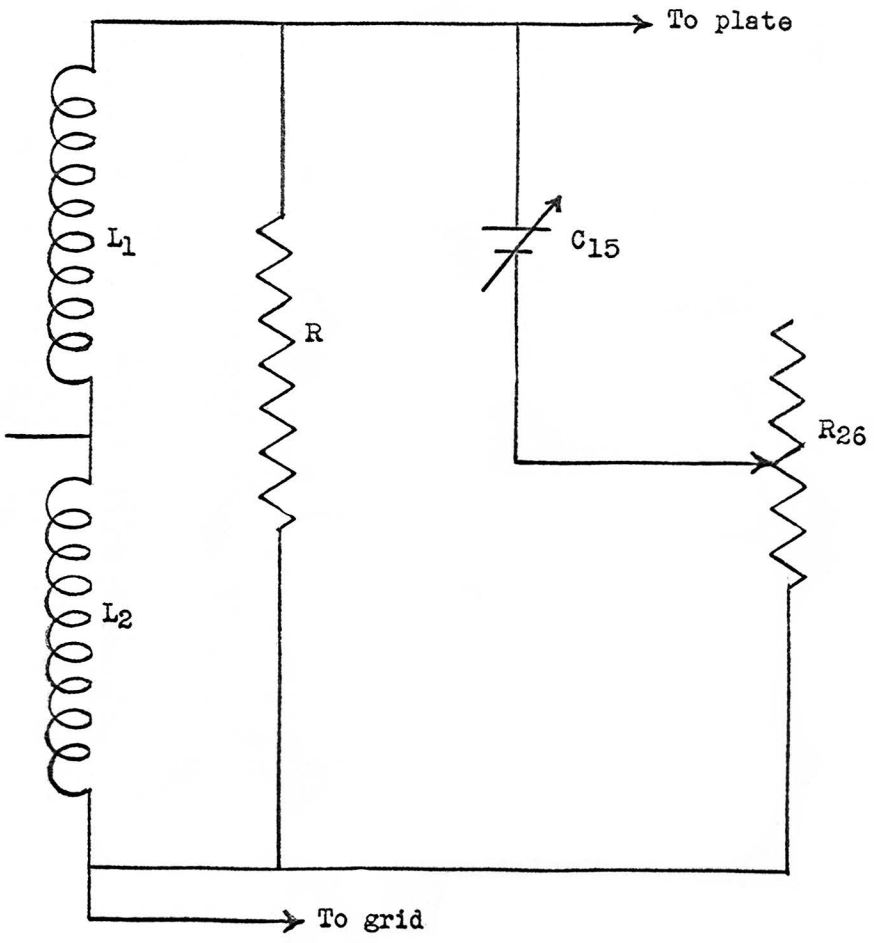

Fig. 16. Tank circuit of oscillator.

choice of either of these capacitors.

A total of five air wound coils, each mounted on a plug-in unit, were used singly with either of the above mentioned capacitors. Each coil was divided by a center tap to form the corresponding plate inductor, L_1, and grid inductor, L_2, as shown in Figure 16. The use of the five inductors with either of the two capacitors gave an almost continuous range of frequencies from 500 kilocycles per second to 18 megacycles per second.

The dimensions, total inductance, number of turns on the grid and corresponding inductance, number of turns on the plate and corresponding inductance, of the five coils used are listed in Table IV. The first three coils were obtained commercially, while the last two coils were hand wound. In Table V are the calculated frequencies found by use of equation (4.3) for the various coils along with the experimentally determined frequencies. The calculated frequencies were evaluated by using the largest and smallest values of each of the two variable capacitors with each of the five inductors. The experimental frequencies are tabulated in terms of the widest range of frequencies found for pulse heights below 400 volts peak to peak, for each coil with each of the two variable capacitors.

As can be seen from Table V, the experimental frequencies lie close to the range of the frequencies calculated by the use of equation (4.3). Experimentally, it was found that the whole range of the variable capacitors would not always produce oscillations. This was thought to be due to an unfavorable feed back ratio, that is, the ratio of the number of turns on the grid inductor to the number of turns on the plate inductor.

Coil	Dimensions of Coil	Total Inductance	Turns on Grid	Grid Inductance L_2	Turns on Plate	Plate Inductance L_1
I	10" long 3" diameter 80 turns	127 mh	8	8.9 mh	72	114 mh
II	10" long 1-1/4" diameter 80 turns	23.3 mh	8	.16 mh	72	21 mh
III	3" long 1" diameter 30 turns	6.47 mh	3	.32 mh	27	5.8 mh
IV	3-1/4" long 1" diameter 20 turns	2.7 mh	3	.06 mh	17	1.95 mh
V	1-1/4" long 1" diameter 7 turns	.72 mh	2	.14 mh	5	.43 mh

Table IV. Inductance coils.

	Calculated Frequency				Experimental Frequency	
Coil	frequency for C_{15}--- 20 mmf	frequency for C_{15}--- 135 mmf	frequency for C_{15}--- 66 mmf	frequency for C_{15}--- 1700 mmf	frequency range for small capacitor	frequency range for large capacitor
I	1.8 MC/sec	.610 MC/sec	.93 MC/sec	.178 MC/sec	1.0 MC/sec to 1.3 MC/sec	.50 MC/sec to 1.2 MC/sec
II	4.0 MC/sec	1.5 MC/sec	2.16 MC/sec	.420 MC/sec	2.4 MC/sec to 3.8 MC/sec	1.3 MC/sec to 3.0 MC/sec
III	7.2 MC/sec	2.8 MC/sec	4.0 MC/sec	.815 MC/sec	4.7 MC/sec to 7.15 MC/sec	4.0 MC/sec to 6.1 MC/sec
IV	12.6 MC/sec	4.85 MC/sec	7.0 MC/sec	1.37 MC/sec	7.7 MC/sec to 11.0 MC/sec	6.7 MC/sec to 9.5 MC/sec
V	24.0 MC/sec	9.1 MC/sec	13.2 MC/sec	2.56 MC/sec	12.5 MC/sec to 18.0 MC/sec	10.0 MC/sec to 16.6 MC/sec

Table V. Experimental and calculated frequencies for five coils.

Detailed experimental work on the last two coils yielded information on the importance of the feed back ratio. Many combinations were tried and two conclusions were drawn. First, if the number of turns on the grid was too small, there was no pulsed oscillation. Second, if the number of turns on the grid was too large, the oscillator would feed back to the pulser, destroying the control over the repetition rate. As was suggested by Skudrzyk (23) a feed back ratio range from 1/6 to 1/20 was found to give the best results.

With coil number V, it was found that no matter what feed back ratio was used, there were pulses which did not destroy control over the repetition rate and those that did. This combination was a function of the setting of the attenuator and the frequency, determined by the setting of the variable capacitor. The frequency range given in Table V for coil V includes only those frequencies where control over the repetition rate was obtainable.

For the last three coils, there was not a one to one correspondence between the pulse width produced by the pulser, and the pulse width of the output of the oscillator. The pulse width of the oscillator was always shorter than the pulsed produced by the pulser. It appeared that the time of shortening on the pulsed oscillation was the time necessary for the voltage to be applied to the oscillator tube, before it would begin its oscillations. To obtain pulses of longer duration, the pulse width was adjusted by use of the controls of the multivibrator.

The capacitor labeled C_{14} in the oscillator circuit shown in Figure 15, has its value dependent on the frequency. As described by Skudrzyk (23), the time constant $R_{24}C_{14}$ is of some importance, for

if this time constant is too large or too small, blocking may occur, causing the pulse to appear sinusoidally modulated. To eliminate the possibility of this occurring, Skudrzyk (23) states that C_{14} should be greater of equal to $20/(fR_{24})$. Each plug-in coil used was equipped with its own C_{14} capacitor which is listed in Table VI, along with the value of $20/(fR_{24})$ for the lowest and highest frequency attainable for a desired coil. As can be seen from Table VI, the values of C_{14} satisfied the above conditions. Experimentally no difficulity was encountered, indicating that a proper choice of capacitance had been made.

The ultrasonic pulse generator was found to work very satisfactorily for the experiment attempted here. Smaller inductors were experimented with to try to obtain frequencies in excess of 18 megacycles per second, but without success. For frequencies to exceed that of 18 megacycles per second, it is suggested that smaller capacitors, smaller coils, and consideration of the redesign of the circuity with regard to assembling of the components be made.

Because the output of the ultrasonic generator was approximately 1,000 volts peak to peak, an attenuator was installed in the oscillator to reduce the output to the range from 150 to 400 volts peak to peak. This was necessary to insure amplitude independent strains in the sample and to insure against fracture of the quartz crystal as mentioned in the EXPERIMENTAL TECHNIQUES section.

The attenuator consisted of a ten position switch and nine one watt resistors. Experimentally it was found that the attenuated voltages for the different positions of the switch were affected by the frequency at which the oscillator operated. At higher frequencies,

Coil	C_{14} Capacitor Used	Lowest Experimental Frequency f_l	Highest Experimental Frequency f_h	$20/(f_l R_{24})$	$20/(f_h R_{24})$
I	4×10^{-9} farads	.50 MC/sec	1.3 MC/sec	1.3×10^{-9} farads	5.14×10^{-10} farads
II	1.5×10^{-9} farads	1.3 MC/sec	3.8 MC/sec	5.14×10^{-10} farads	1.75×10^{-10} farads
III	1.8×10^{-9} farads	4.0 MC/sec	7.15 MC/sec	1.67×10^{-10} farads	9.3×10^{-11} farads
IV	1.8×10^{-9} farads	6.7 MC/sec	11.0 MC/sec	9.95×10^{-11} farads	6.06×10^{-11} farads
V	1.0×10^{-9} farads	10.0 MC/sec	18 MC/sec	6.66×10^{-11} farads	3.7×10^{-11} farads

Table VI. Calculated and experimental values of C_{14}.

there was a marked attenuation of the pulse as compared to that of lower frequencies. This effect was due to the close proximity of the resistors in the switch, inducing an effective capacitive and inductive coupling of these components which depended directly on the frequency.

The attenuator installed in the oscillator was used with an external attenuator to reduce the output of the oscillator to 1/2 volt peak to peak to test the mixing circuit. As was explained in the EXPERIMENTAL TECHNIQUES section, a mixer circuit was constructed to use in conjunction with the amplifier because of its loss of gain above 1 megacycle per second. The schematic for the mixing circuit (26) is shown in Figure 17 while the values of the components are given in Table VII. The 150 volts D. C. was supplied by two 75 volt batteries connected in series, while a 6 volt D. C. battery supplied the heater voltage of the 6AK5. Since the amplifier was sensitive to low frequencies, it did not discriminate against A. C. ripple. Hence batteries were used to eliminate the ripple always present in electronic power supplies.

These 1/2 volt pulses were successfully mixed for all frequencies from 5 to 16 megacycles per second.

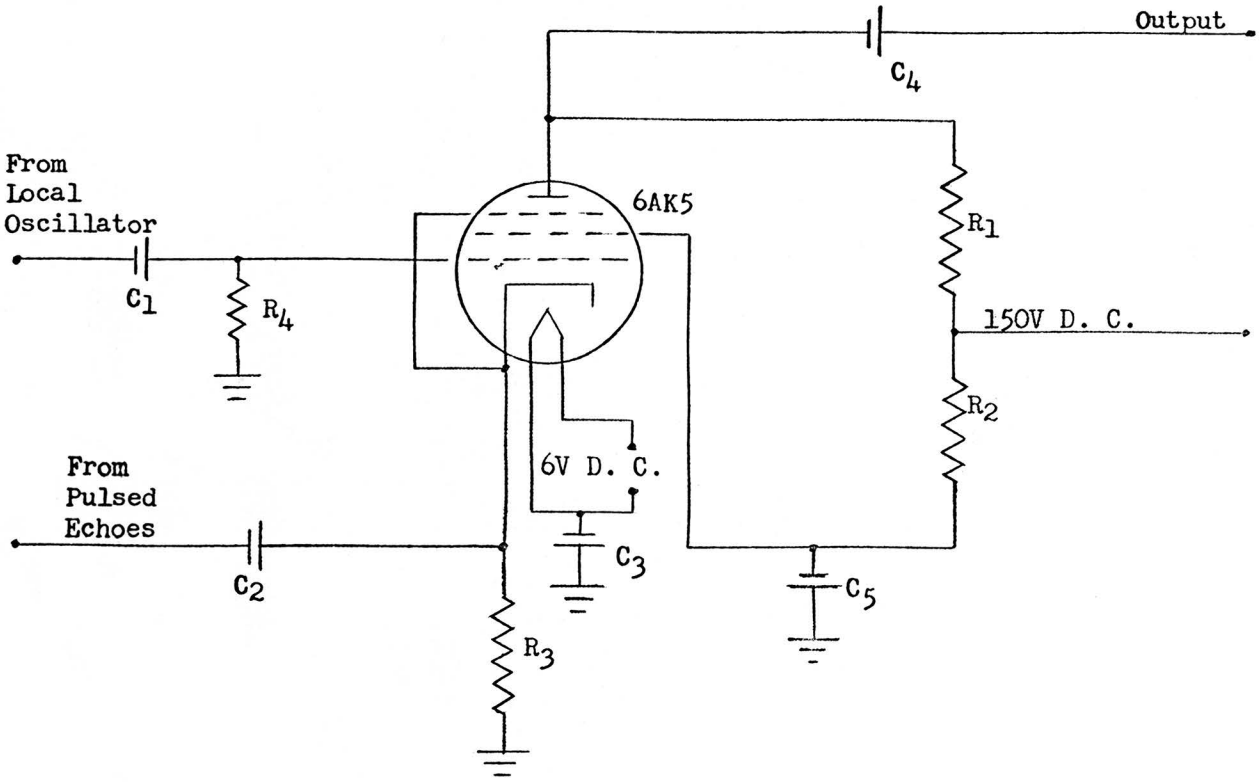

Fig. 17. Mixer circuit.

R_1- 27,000 ohms

R_2- 4,700 ohms

R_3- 560 ohms

R_4- 10,000 ohms

C_1- 40 mmf

C_2- 0.0022 mf

C_3- 0.047 mf

C_4- 0.02 mf

C_5- 0.038 mf

Table VII. Values of components for mixer circuit.

V. EXPERIMENTAL RESULTS

Echoes from the single crystal of aluminum were observed on the oscilloscope for frequencies of 1.0, 1.2, 1.5, 1.8, 2.2, 2.7 and 3.3 megacycles per second. Drawings of the photographed echoes are shown in Figures 18, 19, 20, 21, 22, 23 and 24. The echoes, as photographed, were not as distinct as the lines indicated in Figures 18 to 24, but appeared to have a width greater than expected. This appeared to be caused by trailing pulses which seemed almost as large as the return signal of the desired echo. For the 3.3 megacycle transducer, the photograph was not very distinct because of the low gain of the amplifier at this frequency. Although pulses were observable, only the main envelope of the decay was actually plotted for this frequency. The echoes in this case were just a little larger than the noise of the amplifier.

It will be noted in the diagrams that all the echoes shown were not spaced uniformly as would be expected. The actual time for the trip down the single crystal and back was expected to be in the order of 40 microseconds. In some cases, the echoes appeared to be separated by about this value; and, at other times, the only echoes which could be distinguished above the noise of the amplifier appeared to be separated by times longer than 40 microseconds. The other echoes were assumed to be indistinguishable in the noise level of the amplifier.

It was attempted to excite the harmonics of the transducer, but no results were obtainable. This was thought to be due to any or a combination of three reasons. First, there was the possibility that the harmonics were not excited at all. Secondly, if the harmonics were excited, the return echoes may have been too small to re-excite the

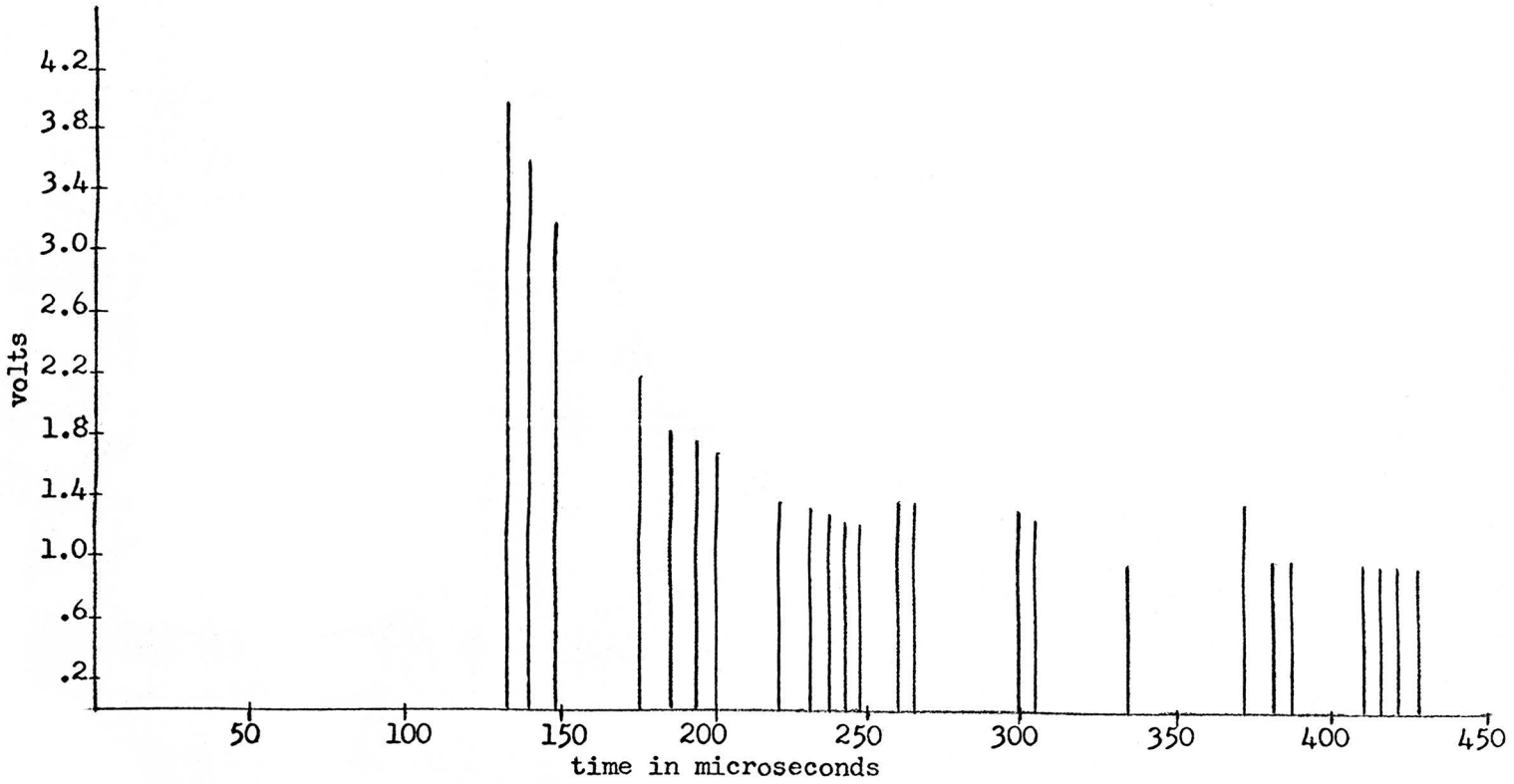

Fig. 18. Echoes obtained for a 1.0 megacycle pulse.

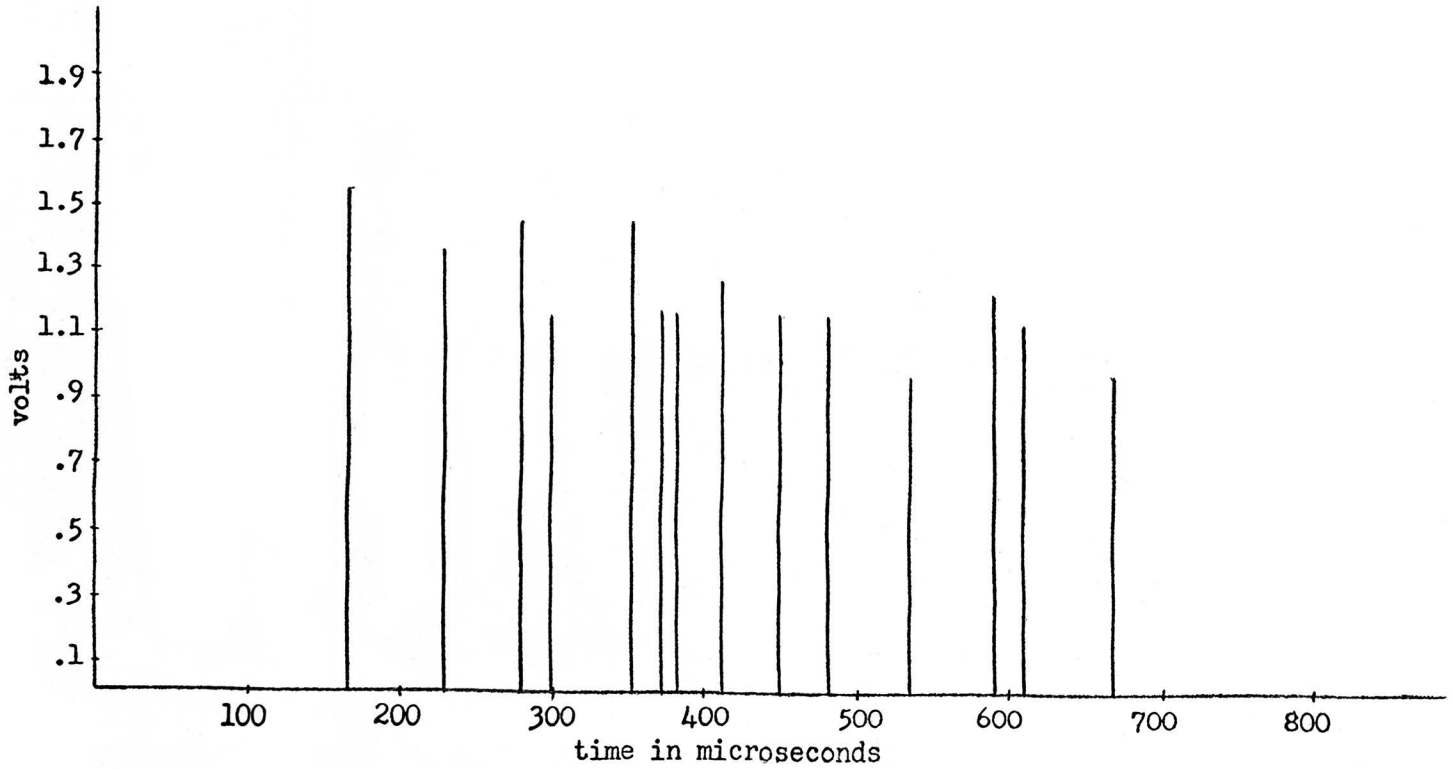

Fig. 19. Echoes obtained for a 1.2 megacycle pulse.

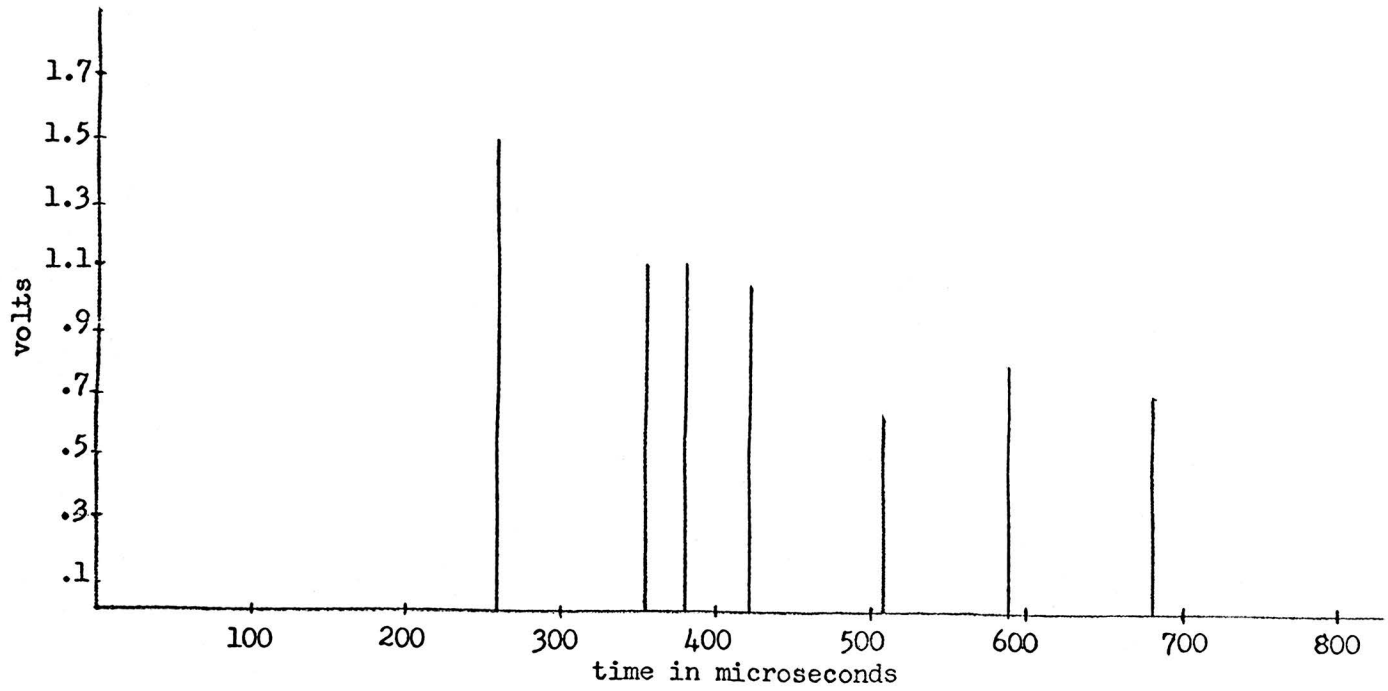

Fig. 20. Echoes obtained for a 1.5 megacycle pulse.

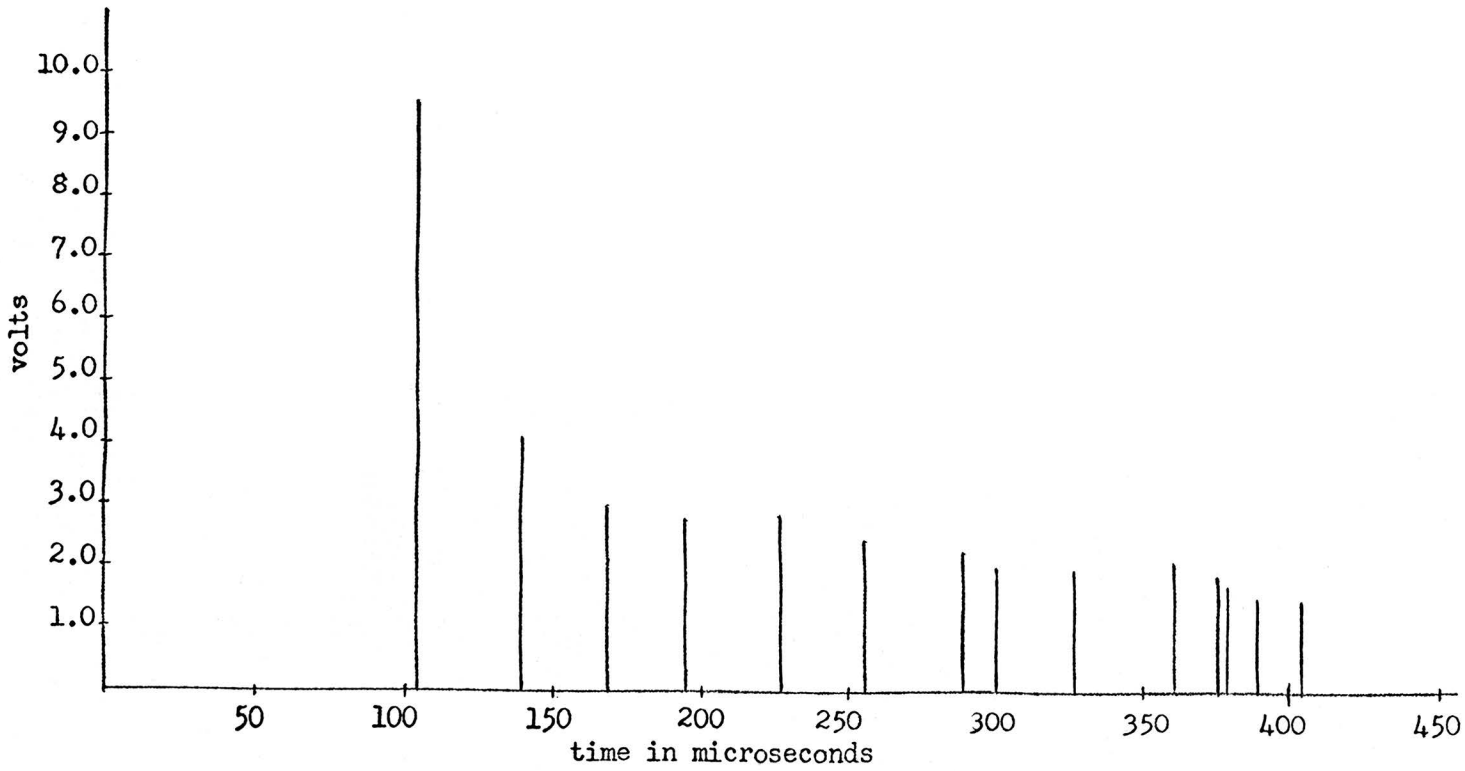

Fig. 21. Echoes obtained for a 1.8 megacycle pulse.

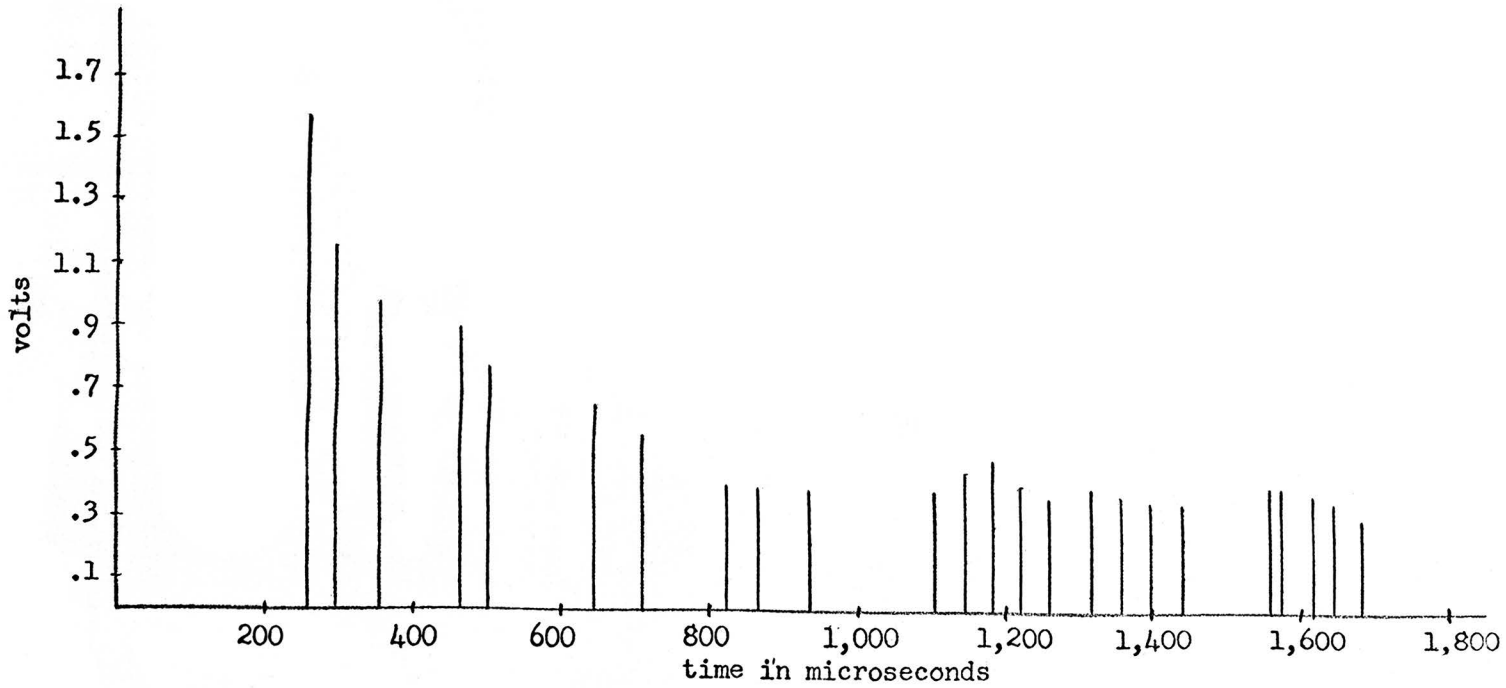

Fig. 22. Echoes obtained for a 2.2 megacycle pulse.

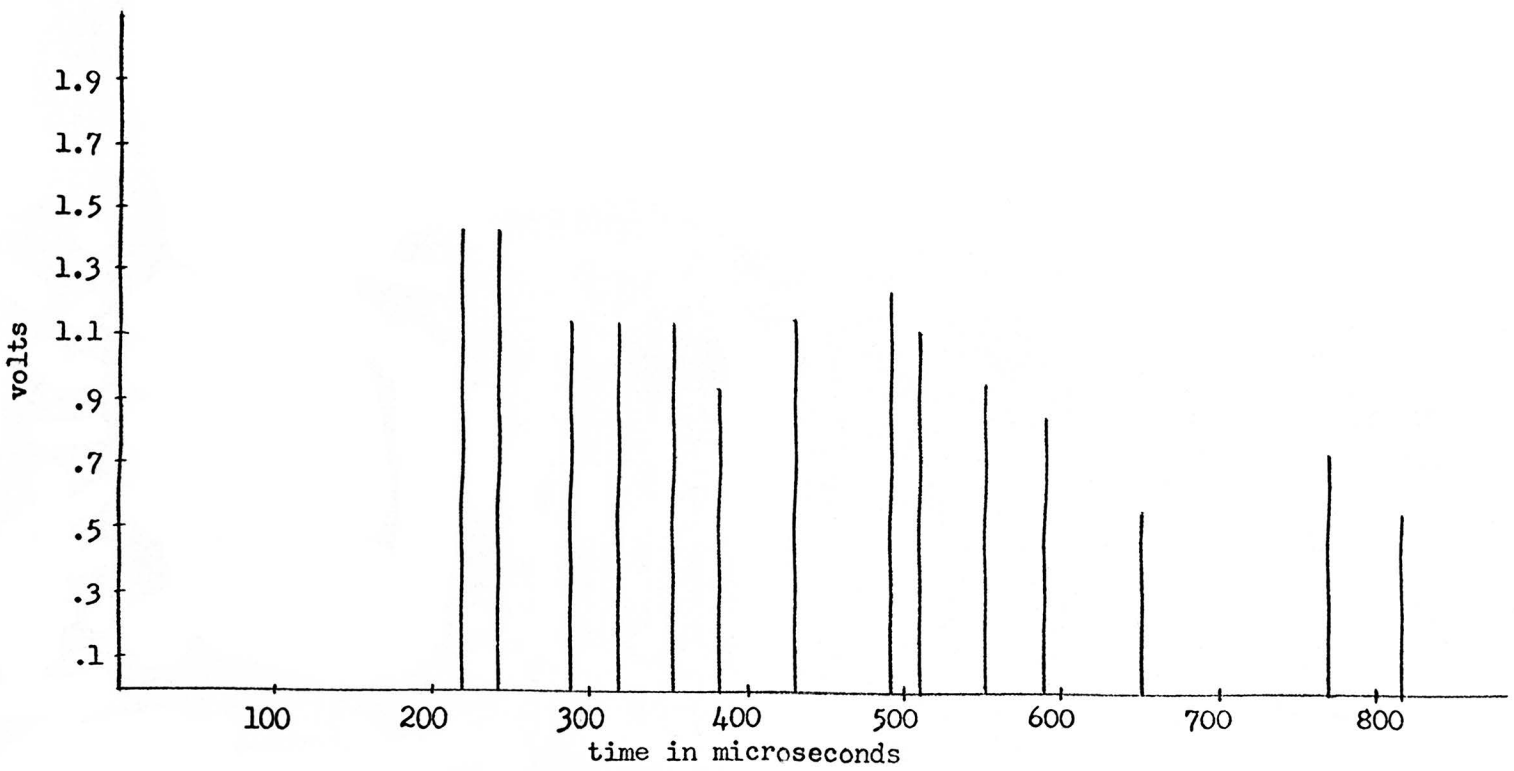

Fig. 23. Echoes obtained for a 2.7 megacycle pulse.

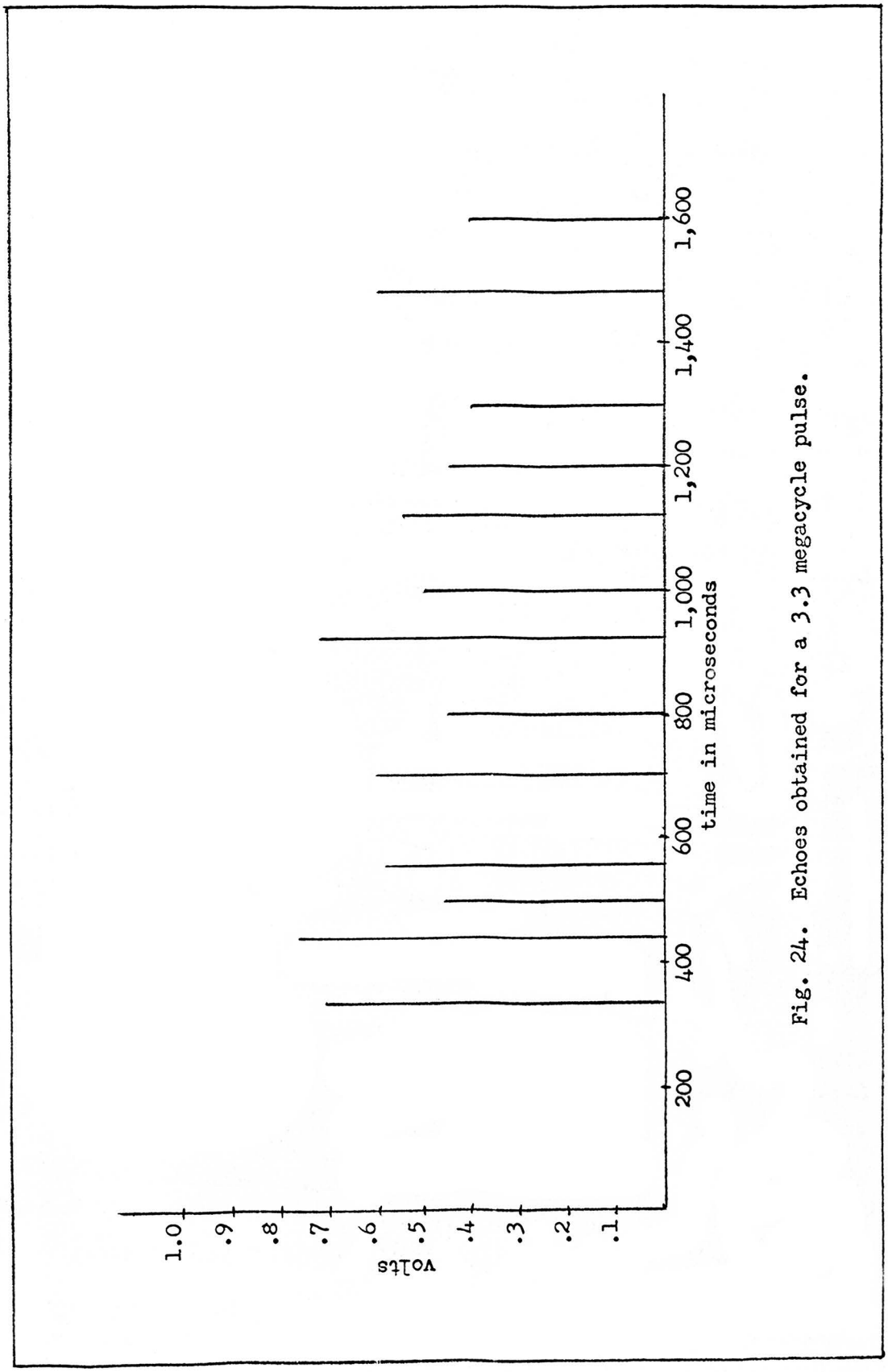

Fig. 24. Echoes obtained for a 3.3 megacycle pulse.

quartz transducer. Third, the mixer may not have been able to mix and detect the small signal returned from the single crystal.

There was a phenomenon which, at first, led to the belief that the harmonics were being transmitted to the sample. The normal response observed on the oscilloscope with the generator detuned from the harmonic frequency was a continuous wave with a frequency of approximately .2 megacycles per second. When the pulse generator was adjusted to within the frequency of the harmonic of interest, there was a definite increase in amplitude of this wave, which decayed exponentially with time. As the decay of the continuous wave resembled the expected decay of the pulsed echoes, it was first though that the echoes from the sample were the cause of the decay pattern. This decay was dismissed as possible attenuation data of the sample for the reasons in the following paragraph.

Because of the relatively high frequencies of the harmonics, the mixer and local oscillator were used to supplement the amplifier as explained in the EXPERIMENTAL TECHNIQUES section. It was observed that the decay pattern discussed above was independent of whether the local oscillator, which fed the mixer, was on or off. Hence, the echoes could not be the cause of the observed decay pattern, for without the local oscillator in operation, the mixer could not produce a pulse in the frequency range where it could be amplified sufficiently to be detected on the oscilloscope. This conclusion was further substantiated when the decay pattern was observed when the signal from the transducer was fed directly to the amplifier.

The final proof that this observed decay pattern was not due to the return echoes of the sample was that this same pattern was observed

when the transducer was placed on a thin sheet of metal.

It was also noted that the frequency response of the decay appeared to be broad as compared to the pulses which were actually obtained at lower frequencies.

With these facts, it was concluded that the observed decay was an electrical ringing produced in the circuit as the harmonic frequencies of the quartz crystals were approached.

As was described in the EXPERIMENTAL TECHNIQUES section, the attenuation in decibels was plotted versus the time (in microseconds) the wave traveled in the specimen in order to determine the attenuation. Although these plots are not shown here, it was found that the points were so scattered that an accurate straight line approximation was impossible. The best straight line approximation possible was made and the logarithmic decrement was plotted against the frequency. The points were so scattered that the data on the attenuation of the single crystal could yield no accurate results.

An examination of the echoes as shown in Figures 18-24 indicates the reasons why the final decrement versus frequency did not yield accurate results. It will be noted in comparing these diagrams that for Figures 18 and 21, the first echo obtained during the time of 100 to 150 microseconds is large compared to the following echoes, giving a good idea of the decay. For the rest of the figures, the echoes were not measurable until after 200 microseconds when most of the decay had already taken place.

The reason why some of the earlier pulses were not observed in some cases was due to the characteristics of the amplifier. After being overdriven by the input voltage, the time required for the

amplifier to return to normal operating conditions varied from 100 to 200 microseconds. An effort was made to reduce this time both by adjusting the controls of the amplifier and by replacing critical capacitors in the circuit itself but with no success. The data shown here was the best obtained.

Another reason why one would not expect this data to yield accurate results was established from Mason (20) in the EXPERIMENTAL TECHNIQUES section. It will be remembered that the criteron for good data was that the sample diameter be twenty times greater than the wave length used. For a one inch diameter crystal as used here, this criteron is obeyed only for frequencies above 5 megacycles per second.

VI CONCLUSION

The experiment conducted here was not successful in obtaining data accurate enough to establish any validity to the theory of Granato and Lücke with respect to measurements of the logarithmic decrement versus the frequency. The main concern with correcting this problem lies mainly in the amplifier. First, the recovery time after being overloaded is too long for this type of experiment. One would like to look at the second echo returning, which would be about 80 micro-seconds after the original pulsed oscillator excites the quartz crystal. Secondly, a very limiting feature of the amplifier was its loss of gain above 1 megacycle per second. To test the Granato and Lücke Theory, one would like to begin at 1 megacycle and work up. The use of a mixing circuit is possible, as tried here, but a broad band amplifier is much more desirable. Third, a gain higher than 4,000 would be even more desirable. For this, of course, one could go to tuned operation of the amplifier (22) which gives gain up to 65,000.

In another sense, this experiment can be considered to be most successful in that the ultrasonic pulse generator was constructed and proved its applicability in research of this type. The experimental frequencies obtained from the pulsed oscillation did lie within the limits of the theoretical calculations.

It was definitely proved that echoes were obtained from the sample which displayed the oscillating characteristics observed by other experimental workers. This method, with improved instrumentation and experimental technique, can prove to be of value in gathering information regarding internal friction and dislocation theory.

VII. BIBLIOGRAPHY

(1) A. Granato and K. Lücke, J. Appl. Phys. 27, 789 (1956).

(2) A. Granato and K. Lücke, J. Appl. Phys. 27, 583 (1956).

(3) D. H. Niblett and J. Wilks, Advan. Phys. 8-9, 1 (1959-1960).

(4) F. Seitz, Imperfections In Nearly Perfect Crystals (Wiley, New York, 1952), p. 40-46.

(5) C. Kittel, Introduction To Solid State Physics (Wiley, New York, 1960), 2nd ed., p. 536-545.

(6) W. T. Read Jr., Dislocations In Crystals (McGraw-Hill, New York, 1953), p. 1-3.

(7) A. Granato and R. Truell, J. Appl. Phys. 27, 1219 (1956).

(8) G. A. Alers and D. O. Thompson, J. Appl. Phys. 32, 283 (1961).

(9) J. Wilks, Phil. Mag. 4, 1379 (1959).

(10) Y. Hiki, J. Phys. Soc. Japan 13, 1138 (1958).

(11) A. Hikata and R. Truell, J. Appl. Phys. 28, 522 (1957).

(12) A. S. Norwick, Phys. Rev. 80, 249 (1950).

(13) Takahaski, J. Phys. Soc. Japan 11, 1253 (1956).

(14) P. G. Bordoni, M. Nuovo, and L. Verdini, Nuovo Cim. 14, 273 (1959).

(15) R. L. Roderick and R. Truell, J. Appl. Phys. 23, 267 (1952).

(16) B. Carlin, Ultrasonics (McGraw-Hill, New York, 1949), 1st ed., p. 63.

(17) A. Granato, R. Truell, and H. Seki, J. Acoust. Soc. Am. 28, 230 (1956).

(18) M. Redwood, Proc. Roy. Soc. (London) 70, 409 (1957).

(19) W. Mason, Piezoelectric Crystals and Their Application To Ultrasonics (Van Nostrand, New York, 1950), p. 409, p. 84.

(20) W. Mason, Physical Acoustics And The Properties Of Solids (Van Nostrand, New York, 1958), p. 44.

(21) J. Lamb and M. Redwood, Proc. Inst. Elect. Engrs. B 103, 773 (1956).

(22) J. Koelling, thesis, Missouri School of Mines and Metallurgy, Missouri, 1963 (unpublished).

(23) E. Skudrzyk, J. Acoust. Soc. Am. 32, 565 (1960).

(24) J. D. Ryder, Electronic Fundamentals And Applications (Prentice Hall, New Jersey, 1959), 2nd ed., p. 569-573.

(25) A. V. Eastman, Fundamentals Of Vacuum Tubes (McGraw Hill, New York, 1949), 3rd ed., p. 443.

(26) The Radio Amateur's Handbook (The American Radio Relay League, Inc., 1962), 39th ed., p. 94.

VIII. VITA

The author was born on June 8, 1939, in St. Louis, Missouri, and received his elementary and high school education in Bayless School District in Affton, Missouri. In September of 1957, he entered Washington University in St. Louis, Missouri, and obtained his B. S. in Engineering Physics in June of 1961.

He entered Graduate School under a graduate assistantship in September of 1961 at Missouri School of Mines and Metallurgy where he completed work for this thesis.